University of California San Diego

Functionalization of RNA-DNA Hybrid Nanostructures by Targeting Abasic Sites with ATMND and Its Derivatives

A Thesis submitted in partial satisfaction of the requirements for the degree Master of Science

in

Chemistry

by

Shudan Yang

Committee in charge

Professor Thomas Hermann, Chair
Professor Simpson Joseph
Professor Jerry Yang

2020

The Thesis of Shudan Yang is approved, and it is acceptable in quality and form for publication on microfilm and electronically:

_____

_____

_____

Chair

University of California San Diego

2020

Table of Contents

LIST OF FIGURES

LIST OF SCHEMES

LIST OF SPECTRA

LIST OF TABLES

ACKNOWLEDGEMENTS

I would first to acknowledge my advisor Professor Thomas Hermann for his invaluable guidance and support throughout my Master thesis project. Whenever I experienced difficulties in either research or school life, he always gave me extremely helpful suggestions and encouragement. It is his warmhearted attitude and patience that made me reap huge benefits from my Masters study. I feel grateful for everyday in his lab.

I would also like to thank Dr. Yongxuan Su (UCSD MS Facility) and Dr. Anthony Mrse for their help with mass spectrometry measurements and NMR training, which contributed to the success of my project.

In addition, I am grateful of Shi Chen and Quint Frauman, thank you for their discussions and advice for my experiments.

Finally, I want to thank Alba Monferrer, a former Master student in the Hermann group. Even though she had already graduated when I started, her research continued to inspire me, pushing forward with my work.

Finally, thank you to all members in Hermann's group.

ABSTRACT OF THE THESIS

Functionalization of RNA-DNA Hybrid Nanostructures by Targeting Abasic Sites with ATMND and Its Derivatives

by

Shudan Yang

Master of Science in Chemistry

University of California San Diego, 2020

Professor Thomas C. Hermann, Chair

DNA self-assembly has been explored as an effective approach for construction of nanomaterials. Previously, research in the Hermann group has established a novel approach to build nanostructures incorporating an L-shaped

RNA connected by DNA strands to self-assemble into hybrid RNA-DNA structures. Abasic sites, as a common lesion in DNA, have been demonstrated to be a target for selective small molecule ligands including the naphthyridine derivative ATMND.

This thesis project investigated ATMND and designed derivatives thereof as ligands targeting the hybrid nanostructures previously developed by Hermann's group and explored selectivity and affinity of abasic site recognition depending on different opposing bases. A strategy of combining two ATMND moieties in one ligand managed to increase the affinity of ATMND-abasic site association. This work demonstrated the feasibility to combine RNA, DNA and small chemical molecules to construct new self-assembled nanostructures which would be further explored their applications, such as porous materials construction or drug delivery, and provided a rational pathway to modify and functionalize composite nano materials.

Introduction

1. Noncovalent modifications of DNA and RNA through abasic site ligands

1.1. AP site

Apurinic/apyrimidinic (AP) site (**Figure 1**), also known as abasic site, is one of the most frequent lesions (damages) in living cells that do not significantly distort the DNA helix structure. It has been suggested that more than 10,000 abasic sites are created through loss of bases per day in one mammalian cell (1).

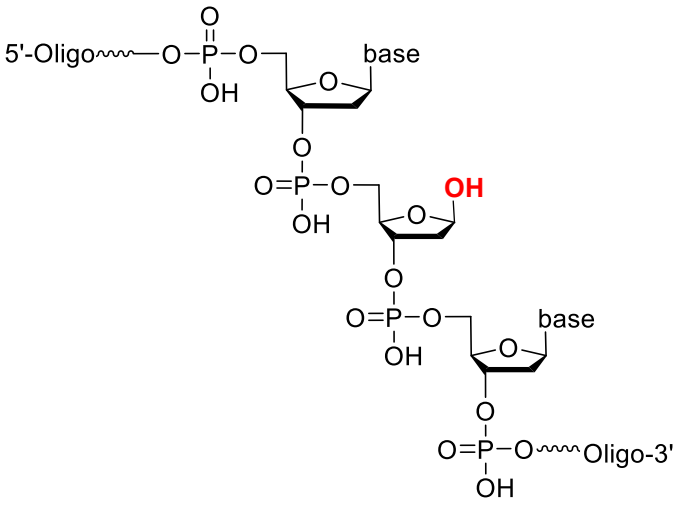

Figure 1. Structure of AP site.

Such loss of base in a DNA single strand may occur spontaneously, as a result of chemicals, radiation or treatment with cytostatic drugs (2), or due to enzyme activities, for instance, DNA glycosylases which initiates base excision repair, recognizing and removing abnormal base, leaving an AP site (3). AP sites are extremely reactive due to its alkali-labile residue left which can open the furanose ring when exposed to a nucleophile and to give free aldehyde and free alcohol (**Figure 2**). DNA single strand breakage occurs catalyzed by AP lyase via β-elimination reaction (4), blocking replication and transcription, and generating

mutagenic and lethal DNA damages. Some representative base lesions are shown in **Figure 2** below.

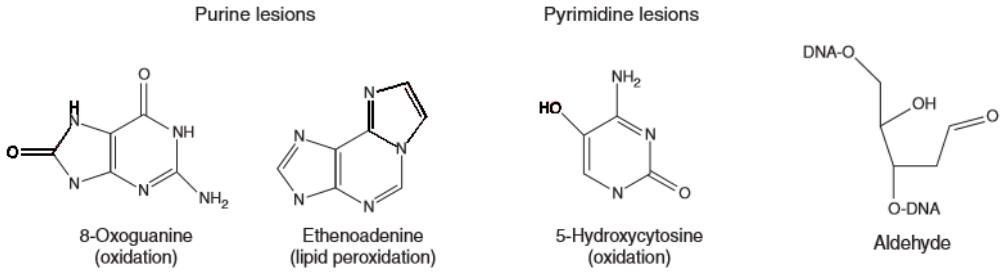

Figure 2. Chemistry of common base lesions and AP site aldehyde (2).

1.2. Nucleic acid noncovalent modification based on AP site binding ligands

Nucleic acids are capable to carry various modifications and employ them to exert essential tasks and assume diverse functions in cellular processes in eukaryotic organisms and applications in nanotechnology, diagnostics and therapeutics. In past decades, many efforts had been devoted to covalent modification of nucleic acids. For example, Wyatt reported methylation of cytosine in genomic DNA and 2′-O-(pyren-1-yl)methyluridine phosphoramidite was introduced as an RNA building block by Yamana and coworkers in 1991 (5).

Recently, research emerged to study non-covalent dynamic pathways to form functional oligonucleotides, which can be broadly utilized in DNA or RNA diagnostics, or reguatio nof gene expression regulations. For instance, incorporation of metal ions, like Ag^+ (6), into nucleic acids by means of metal-mediated base pairs represents an interesting strategy through site-specific introduction of functional molecules into self-assembling supramolecules. One of the advantages is due to the predictable self-assembly, the two- and three-dimensional orientation in space of

these functional sites can be readily controlled (7). Another kind of site-specific decoration of nucleic acids is to attach suitable ligands, enabling the generation of aptamer-ligand complexes. Aptamers are short nucleic acids isolated from *in vitro* experiments named as SELEX (systematic evolution of ligands by exponential enrichment) (8). Aptamers reveal high selectivity and binding affinity toward targets achieved by a combination of molecular shape complementarity, precise stacking of flat moieties and hydrogen bonds. Several ligand classes involved in aptamer-ligand association have been reviewed by Hermann and Patel in 2000 (**Figure 3**): aromatic ligands (**a**), amino acids (**b**), oligosaccharides (**c**), peptides and proteins (**d**). (9)

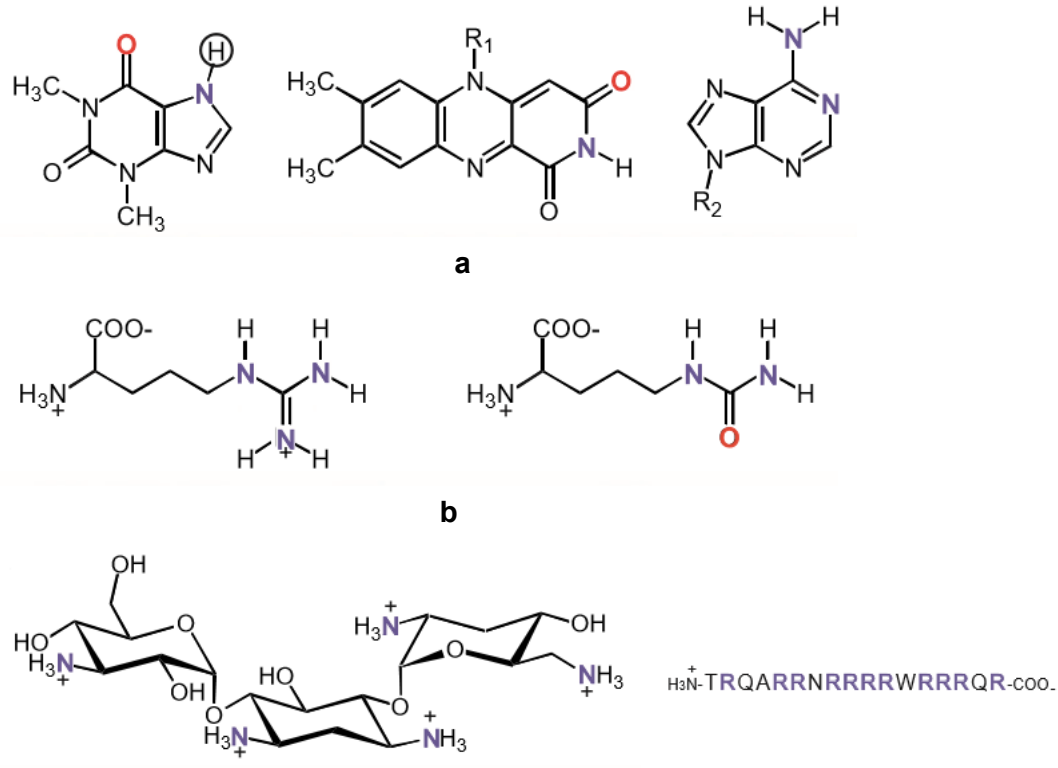

Figure 3. Examples of diverse aptamer-ligands (**a.** flat aromatic systems, **b.** amino acids, **c.** oligosaccharide, **d.** peptide) can be in complex with nucleic acid aptamers.(9)

Over the past ten years, there have been increasing numbers of non-covalently DNA-binding molecules developed as DNA analysis probes or potential drug candidates, such as netropsin, which contains two aromatic N-methylpyrrole rings and targets the minor groove of DNA duplexes, and anthraquinones, which bind to duplex DNA through intercalation (10). In addition to DNA-ligand interactions through groove binding or intercalation, an abasic site (AP site) can serve as a selective cavity for ligand binding. In duplex DNA with AP site, ligands can form pseudo-base pairs with opposite intrahelical orphan nucleobases along the Watson-Crick edge, where the ligand is stacked with two nucleobases flanking the AP site (**Figure 4**). While naturally occurring AP site is one of the most common form of DNA damages, such a lesion site can also be incorporated into synthetic DNA duplexes to test affinity of a ligand with specific nucleobase in a DNA strand. The complementary strand containing AP site is hybridized with the target DNA strand in order to place the AP site at anticipated position. This strategy was also utilized in this project.

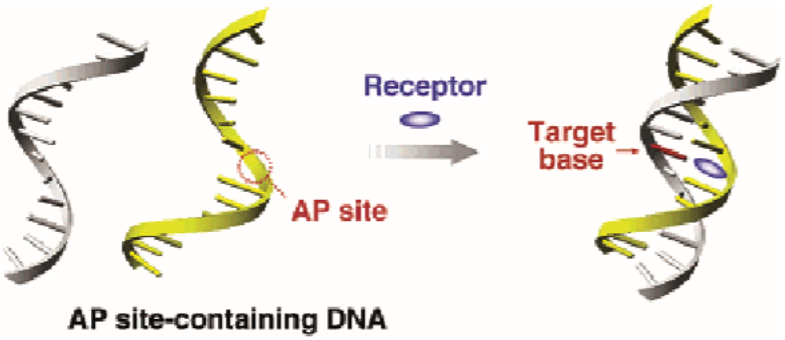

Figure 4. Schematic illustration of nucleobase recognition using an AP site-containing DNA strand. (11)

Recently, a series of aromatic ligands which can selectively bind to nucleobases opposite an AP site with different affinities have been found. Some of those ligands are fluorescent, and have significant potential for applications of fluorescence detection or gene analysis, including amiloride, lumichrome, pteridine, 2-amino-1,8-naphthyridine and their derivatives. Amiloride selectively binds to thymine (12), pteridine trends to guanine (13), alloxazine selectively binds to adenine (14), and riboflavin is selective for thymine (15). Several such ligands are shown in **Figure 5**.

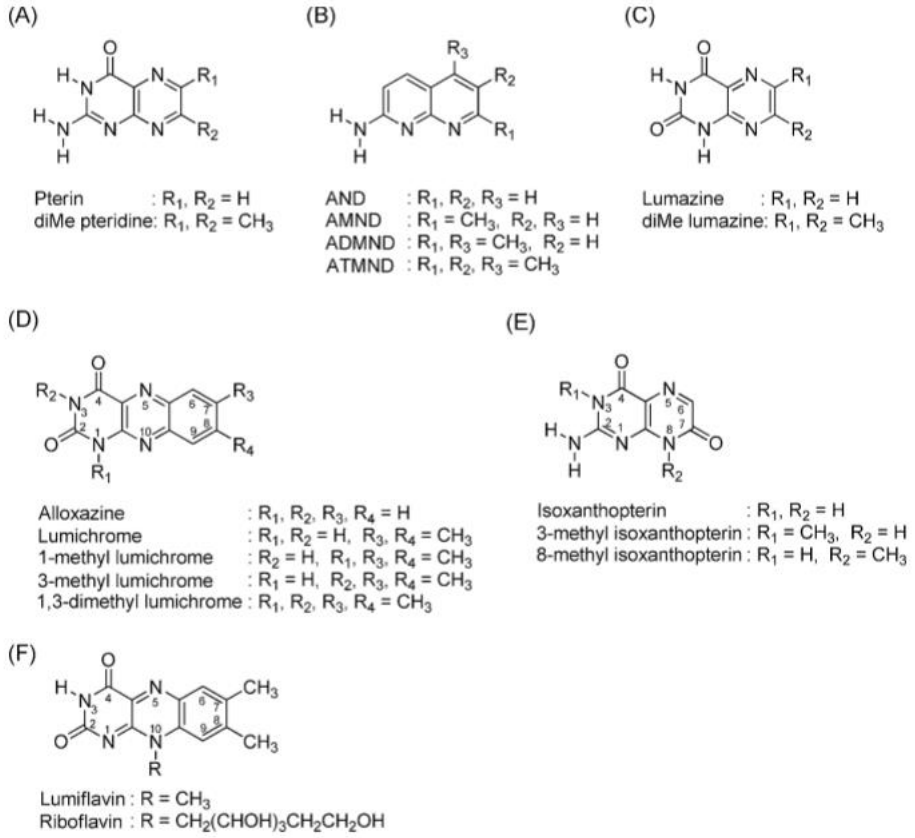

Figure 5. Structures of AP site binding ligands. (A) Pterin and its methylated derivative diMe pteridine. (B) 2-Amino-1,8-naphthyridine (AND), and its methylated derivatives, 2-amino-7-methyl-1,8-naphthyridine (AMND), 2-amino-5,7-dimethyl-1,8-naphthyridine (ADMND), and 2-amino-5,6,7-trimethyl-1,8-naphthyridine (ATMND). (C) Lumazine and its methylated derivative diMe lumazine. (D) Alloxazine and its methylated derivatives. (E) Isoxanthopterin and its methylated derivatives. (F) Structure of flavins. (16)

2-Amino-1,8-naphthyridine and its homologous series (**Figure 6**) have been reported as AP site binding dyes that bind through formation of hydrogen bonds toward opposite nucleobases and stacking interaction with nucleobases flanking AP site. These series of fluorophores showed selectivity for pyrimidine (C, T) over purine (A, G) bases. An isothermal titration calorimetry stud by Yusukye Sato and colleagues revealed that introduction of methyl groups effectively increases binding affinity to cytosine (17). As a result, in this project, I mainly focused on 2-amino-5,6,7-trimethyl-1,8-naphthyridine (ATMND) which was expected to have highest selectivity and affinity to cytosine opposite AP site among these homologous series compound.

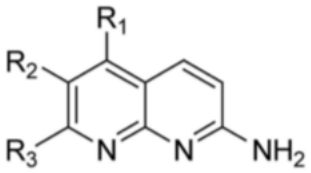

	R_1	R_2	R_3
AND	H	H	H
AMND	H	H	CH_3
ADMND	CH_3	H	CH_3
ATMND	CH_3	CH_3	CH_3

Figure 6. Structures of series of 2-amino-1,8-naphthyridines. (17)

2. Nucleic acid nanostructures

2.1. DNA nanotechnology

Nano-objects made of DNA are becoming promising for various applications in a wide array of fields such as biology, chemistry or pharmaceutical science. DNA, as important building blocks of nanomaterials, has many remarkable advantages over other kinds of constituents of nanostructures, such as its programmable assembly, predictability of 2D and 3D shapes at molecular level, reversibility at different temperature or pH, biocompatibility and its binding abilities to varieties of

targets like practical enzymes or small molecular ligands which make it easy to fabricate and functionalize (18). Owing to these merits, functionalized DNA nanostructures have been used in various biomedical applications. For example, static and dynamic DNA nanostructures serving as delivery vehicles (19). Furthermore, biomacromolecules, like some antibodies, were attached to DNA nanostructures for detection of biomolecules, drug releasing control or gene therapy (20). Diversities of DNA nanostructures including simple tiles (**Figure 7a**) and higher-order structures (**Figure 7b**) have been developed shown in **Figure 7**.

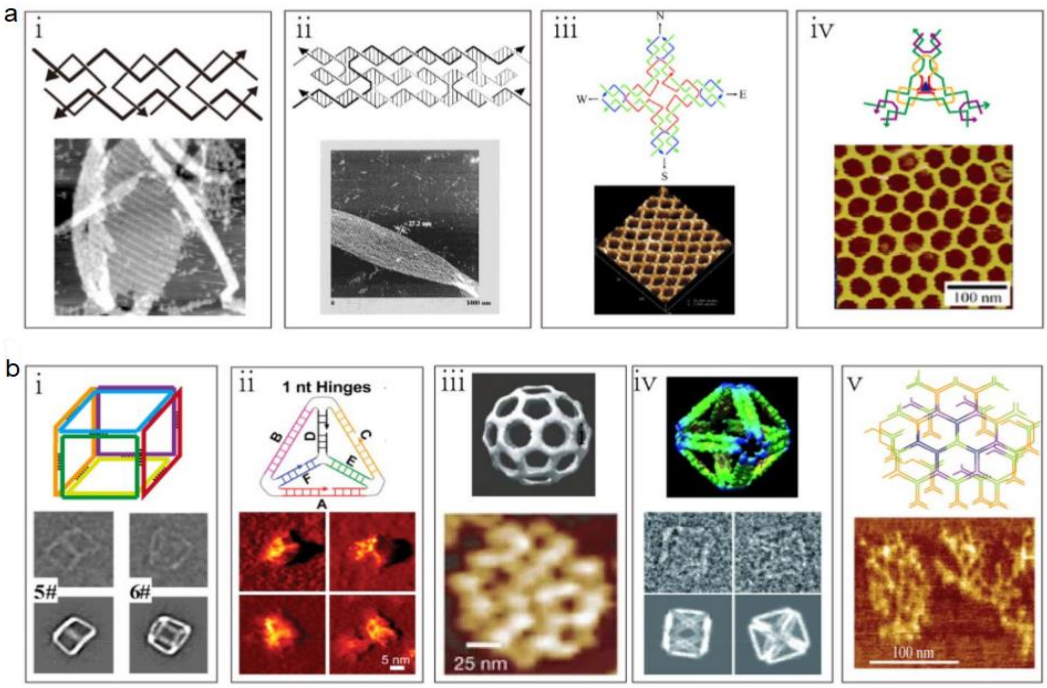

Figure 7. Examples of some DNA nanostructures. **a**. Simple DNA blocks: (i) double-crossover (DX) tiles, (ii) triple-crossover (TX) tiles, (iii) 4×4 tiles, (iv) three-point star tiles. **b**. Higher-order DNA nanostructures constructed from tiles through bottom-up assembly: (i) DNA cube, (ii) DNA tetrahedron, (iii) DNA polyhedron, (iv) DNA octahedron, (v) DNA dendrimer. (18)

2.2. RNA nanotechnology

The field of RNA nanotechnology has developed rapidly in the past few decades. Apart from those similar properties with DNA nanomaterials, increasing

interest of RNA nanoparticles comes from its versatility in structure and function. RNA's ability to adopt varieties of secondary and tertiary structural motifs (**Figure 8**), such as bulges, stems, hairpin, loops and junctions, leads to serving as ideal building blocks to design nanoparticles with diverse size and shapes. Moreover, noncanonical base pairs (G-U, G-A, A-U, etc), base stacking and complicated networks of tertiary contacts enhanced versatility and thermodynamic stability of RNA nanostructures (21).

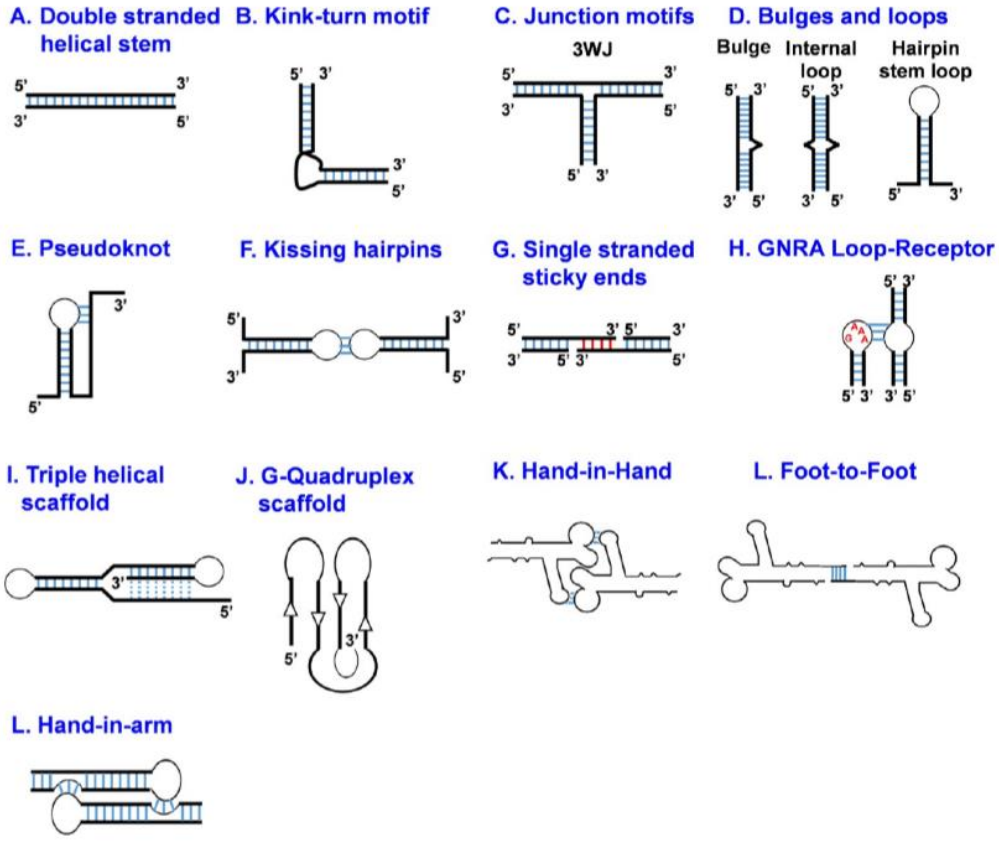

Figure 8. RNA motifs can be used to generate higher-order RNA nanoparticles. (21)

Some naturally occurring RNA motifs were demonstrated to exhibit features of predefined angular geometry, including a pRNA three-way junction (3WJ) motif studied by Guo and colleagues (22), which can adopt angles from 60º to 90º or 108º. Another well-known RNA structural motif with a unique 90º bend is a ligand-

responsive RNA switch module extracted from the subdomain IIa bulge in the internal ribosome entry site (IRES) of the hepatitis C virus RNA genome (**Figure 9**) previously used by Hermann's group to create a self-assembling double-stranded planar nanosquare (23).

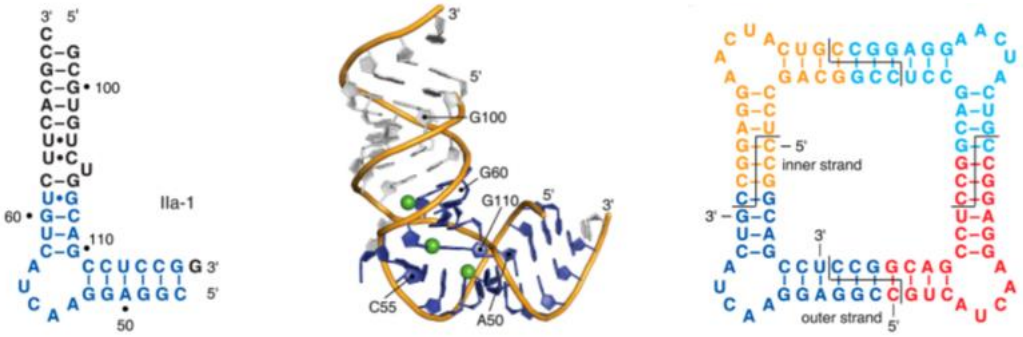

a **b** **c**

Figure 9. **a.** Secondary structure of the IIa-1 RNA representing the subdomain IIa of the IRES from HCV, **b.** three-dimensional structure of the IIa-1 RNA, **c.** secondary structure of the RNA square (the four copies of the IIa-1 core are highlighted in different colors and lines indicate boundaries of oligonucleotides). (23)

2.3. Hybrid RNA-DNA nanoparticles

It is a promising strategy to build self-assembling RNA-DNA hybrid nanoarchitectures from combining programmable building blocks including DNA and RNA modules with rich structural and functional diversities. Despite challenges of rational design and assembly of RNA architectures, several examples have been reported to de novo design RNA containing nanostructures where RNA self-assembly was programmed by DNA molecules. For instance, Ko and colleagues have reported a self-assembling RNA-DNA hybrid double crossover (DX) motif (tile) (24) shown in **Figure 10**, which consisted of two identical RNA strands (R, red), two identical short DNA strands (S, black) and a long two-times repetitive DNA strand (L2, green).

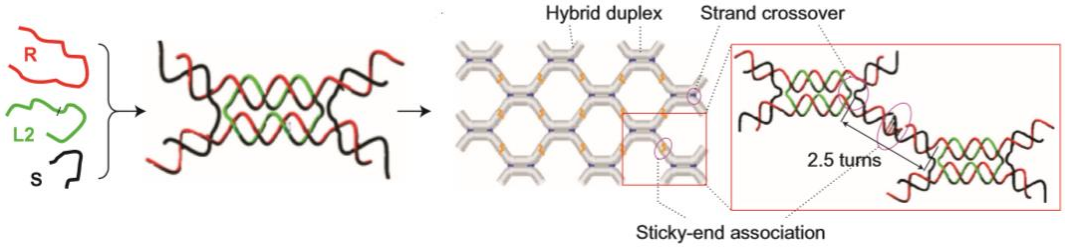

Figure 10. DNA-programmed RNA self-assembly: an RNA-DNA hybrid double crossover (DX) motif (tile). (24)

2.4. Previous work in Hermann's group on RNA-DNA hydrid nanostructures

Hermann's group constructed self-assembling RNA-DNA hybrid nanostructures using an L-shaped planar RNA corner and DNA connectors with asymmetric complementary overlapping sequences as building blocks (**Figure 11a**). Asymmetric overlapping sequences were designed to avoid forming self-complementary squares like the previously designed all-RNA square (**Figure 9c**) (25).

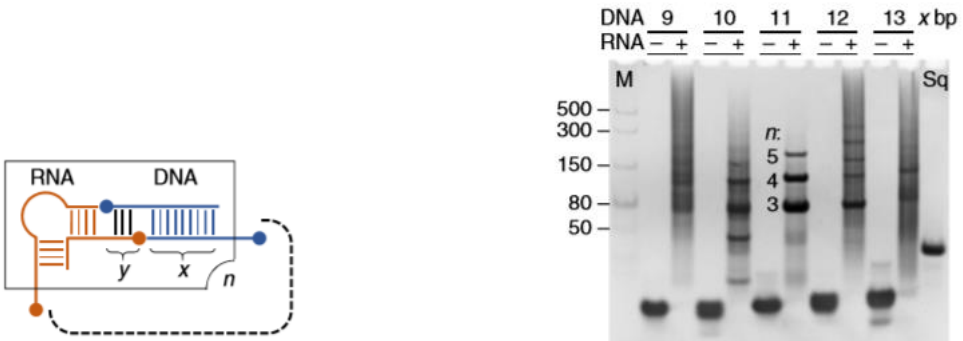

a **b**

Figure 11. Design and screening strategy for RNA-DNA hybrid nanoshapes. **a.** Design of polygonal RNA-DNA hybrid nanoshapes that contain bent RNA motifs as architectural joints and straight DNA modules as connectors. Length variation of single-stranded regions (y) for interaction between the building blocks, length of the double-stranded core (x) of the DNA modules. **b.** Screening for stable hybrid complexes of RNA and DNA module combinations by native polyacrylamide gel electrophoresis (PAGE). (25)

Since the hybrid structure can only form if the DNA double helix ends in a complete turn and aligns the end in the same plane, the lengths of DNA between RNA corner were screened through native PAGE (**Figure 11b**). The best DNA module tested was one with 11 base pairs which gave three different stable hybrid structures. These three species were extracted from gel and shown to be triangle, square and pentagon nanoshapes by atomic force microscopy (AFM) (**Figure 12**). (25)

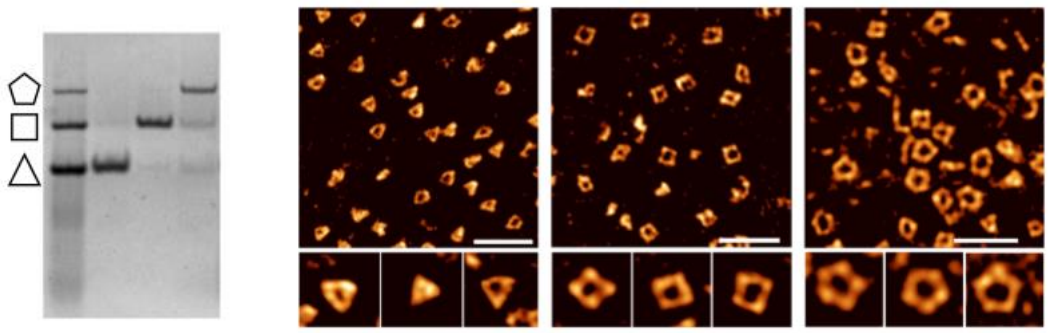

a **b** **c** **d**

Figure 12. Isolation and imaging of RNA-DNA hybrid nanoshapes. **a.** Native PAGE analysis of polygonal RNA-DNA-11 (2-11) hybrid nanoshapes. **b-d.** AFM imaging of homogenous populations of **b.** triangles **c.** squares **d.** pentagons obtained by extraction of individual bands from the gel. Scale bars represent 50nm. Inserts with individual nanoshapes are 30nm wide. (25)

3. Objectives

The main object of this project is to introduce small molecules into self-assembled RNA-DNA hybrid nanostructure built by Hermann's group and to construct nanoshapes incorporating RNA corners, DNA modules and small chemical compounds. DNA modules with abasic sites are used as building blocks to generate hybrid nanostructures following the methods reported by a previous student Alba Monferrer. As a ligand targeting the AP sites, I focused on ATMND and its derivatives.

The first part of this work includes fluorescence detection of ATMND binding to AP site opposite different base. AP site-containing DNA duplexes identified through fluorescence screening were combined with L-shaped RNA modules to build nanostructures. Then, binding of ATMND to AP site-containing self-assembly RNA-DNA hybrid nanoshapes was studied (**Figure 13a**).

The second part of my work aimed at the design and synthesis of ATMND derivatives with larger and more complex structures and studies of their interaction with nanoshapes, ATMND here serves as a joint (**Figure 13b**), which seems like a promising strategy to functionalize these novel nano materials. The stability of such interaction can be detected by FRET experiments.

The third part of my work is to design and synthesize a ligand dimer which combines two ATMND moieties linked by a long enough linker. Binding of ATMND dimer to abasic sites within the same nanoshape (**Figure 13c**) was studied through native PAGE.

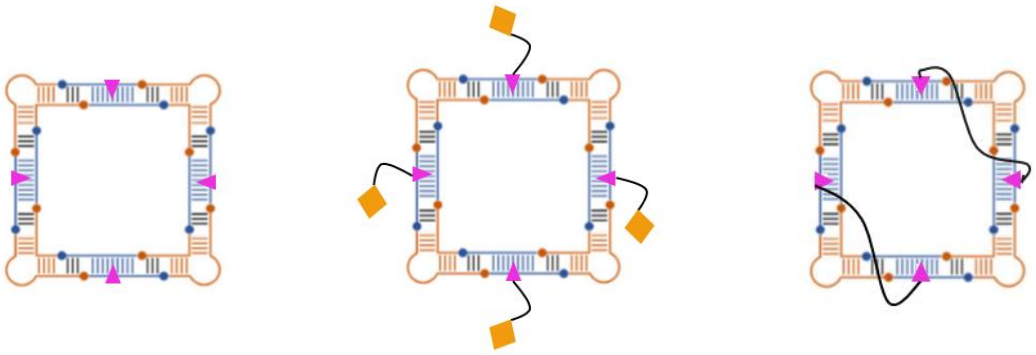

a **b** **c**

Figure 13. Design of functionalized nanosquare incorporated with **a**. ATMND, **b**. ATMND derivative, **c**. ATMND dimer (blue stands for RNA corners, red stands for DNA modules, pink represents ATMND ligand which link with functional groups (orange) or another ATMND through alkyl linkers (black)).

Results and Discussion

1. Synthesis of ATMND and exploration of its affinity to AP site-containing DNA duplexes and hybrid RNA-DNA nanostructures

1.1. Synthesis of ATMND

ATMND (2-amino-5,6,7-trimethyl-1,8-naphthyridine) **1**, as a small fluorescent molecule, has been reported to be able to strongly bind to cytosine (26) and thymine (27) opposite to an abasic site in DNA duplexes to form a complex, resulting in quenching of its fluorescence. ATMND quenching mainly based on static quenching mechanism when it inserts into AP site and stacked by both flanking nucleobases. ATMND compound is synthesized according to a pathway to prepare naphthyridines from the literature (28), starting with electrocyclic ring closure by heating a mixture of 2,6-diaminopyridine **2** and 3-methylpentane-2.4-dione **3** in phosphoric acid (**Scheme 1**).

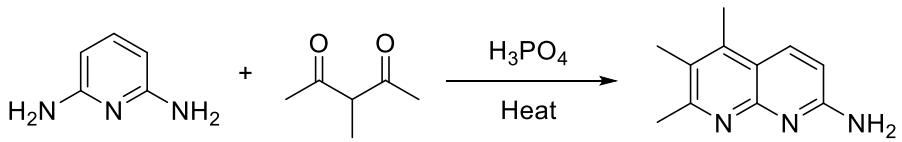

2 **3** **1**

Scheme 1. Synthesis of 2-amino-5,6,7-trimethyl-1,8-naphthyridin (ATMND) **1**.

The mechanism is similar to a Conrad-Limpach Condensation, in which 2,6-diaminopyridine functions as an electron donor, carbonyl group serves as the electron acceptor (29), followed by removal of H_2O and a series of proton transfers.

1.2. Interaction studies of ATMND with AP site-containing DNA duplexes

Prior to the standard detection, the concentration of ATMND was optimized first to achieve the best assay performance. As shown in **Figure 14**, with an

increasing in ATMND concentration, the fluorescence signal of ATMND increased. In hope of acquiring a robust fluorescence signal with the least amount of material, I chose 1 μM of ATMND as the optimal concentration used in the following experiments.

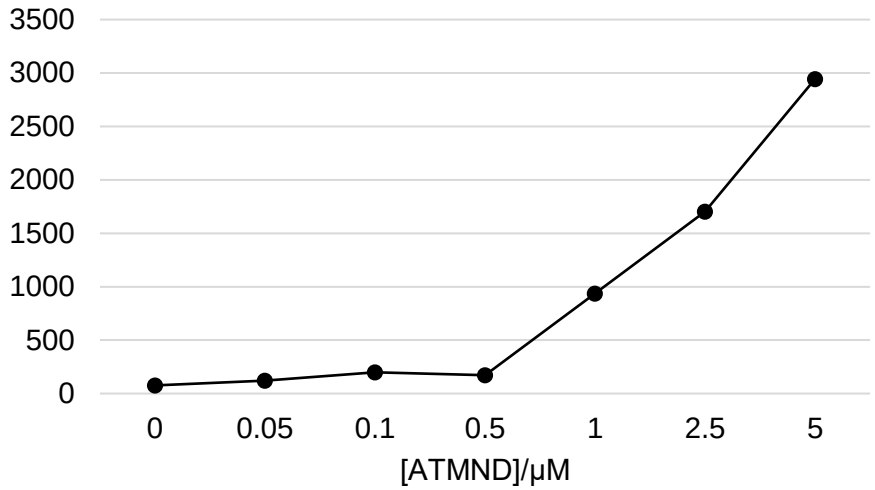

Figure 14. Optimization of ATMND concentration for fluorescence experiments.

The binding properties of ATMND to AP site-containing duplexes with different bases opposite AP site were firstly examined by fluorescence studies. In order to get a comprehensively quantitative understanding of the affinity of ATMND to the four possible bases opposite AP site, a fluorescence titration was done with constant concentration of ATMND as 1 μM dissolved in DMSO and increasing concentration of 23-meric AP site-containing DNA duplexes (5'-CCT CGG ACG TG**X** CGA TA CGA GAC-3'/3'-GGA GCC TGC AC**N** GCT AT GCT CTG-5', **X**=AP site, **N**=T, A, C or G) from 0 μM to 10 μM, dissolving in 10 mM sodium cacodylate buffer (pH 6.5) with 2 mM magnesium chloride at room temperature. ATMND exhibited an emission band acquired at 440 nm when excited at 375 nm and a cut off filter set at 420 nm. The result, as shown in **Figure 15**, proved that the emission of ATMND quenched

significantly in the presence of DNA duplexes with pyrimidine bases (**N**=T or C) opposite AP site, but moderately in the DNA duplexes with purine bases (**N**=A or G) opposite AP site. This result was in accordance with the reported fluorescence responses of ATMND binding to AP site. Since cytosine proved to have the best binding capacity with ATMND at AP site, replication of this group (**N**=C) was done. A binding curve was fitted with averaged data points, and an EC50 value calculated at 0.67 μM. Curves of ATMND binding to other three bases (**N**=T, A, G) were calculated from single sets of data points.

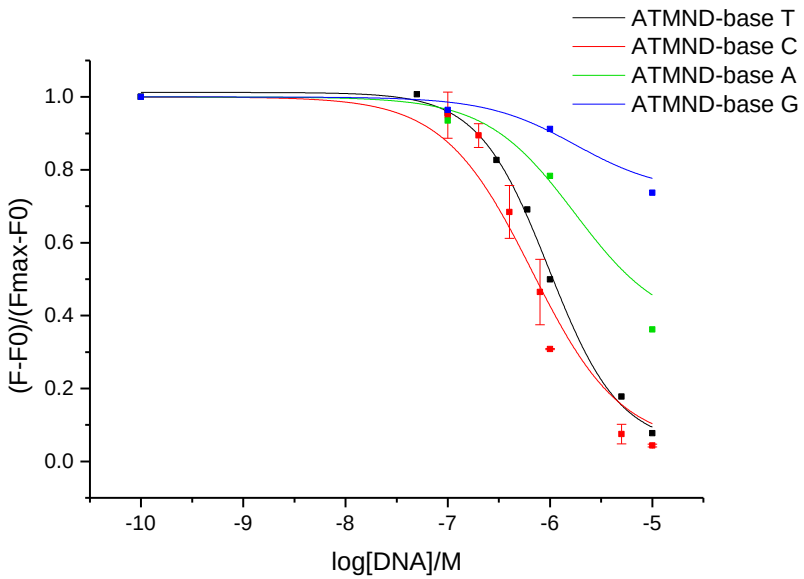

Figure 15. Fluorescence responses of ATMND (1 μM) to target nucleobases (**N**=T(black), A(green), C(red) or G(blue)) in 23-meric AP site-containing DNA duplexes in solutions buffered to pH 6.5 (10 mM sodium cacodylate) and containing $MgCl_2$ 2 mM. Excitation: 375 nm, emission: 440 nm, cut off at 420 nm. *T*=room temperature. Duplexes: 5'-CCT CGG ACG TG**X** CGA TA CGA GAC-3'/3'-GGA GCC TGC AC**N** GCT AT GCT CTG-5', **X**=AP site, **N**=T, A, C or G.

1.3. Interaction studies of ATMND with AP site-containing hybrid RNA-DNA nanostructures

Since ATMND has been demonstrated to bind selectively to AP opposite to

cytosine at highest affinity in AP site-containing duplexes according to the fluorescence titrations showed in **Figure 15**, it is also expected to strongly bind to cytosine opposite AP site in hybrid RNA-DNA nanostructures developed in our lab. In order to examine this hypothesis, 2-11 nanostructures shown in **Figure 12** were used to replace DNA duplexes for fluorescence titration, any other conditions and procedures are the same. Nucleotide sequences of repeating segment in nanostructures used are shown in **Figure 16**.

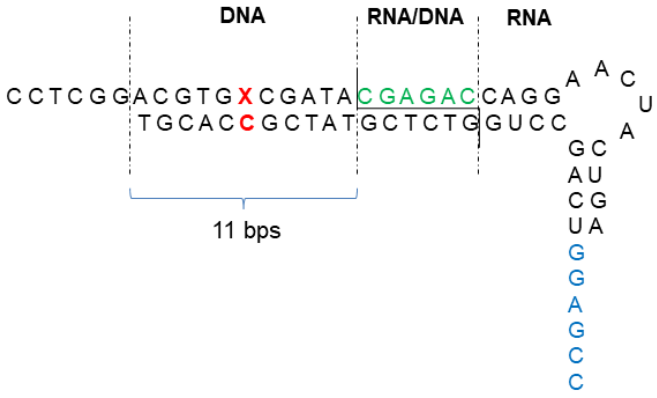

Figure 16. Repeating segment of 2-11 nanostructures build with two RNA strands and two DNA strands.

Fluorescence quenching was clearly observed with increasing concentration of nanoshapes containing AP site opposite cytosine compared with adding nanoshapes without AP site, which indicates that ATMND can also be inserted and quenched at AP site-containing 2-11 nanostructures (**Figure 17**).

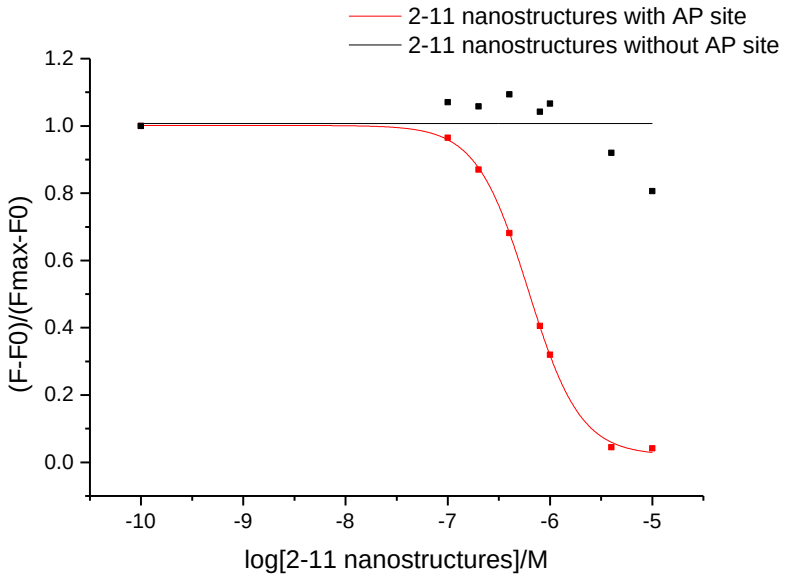

Figure 17. Fluorescence responses of ATMND (1 μM) to target nucleobases cytosine in 2-11 nanostructures (**X**=AP site) in solutions buffered to pH 6.5 (10 mM sodium cacodylate) and containing $MgCl_2$ 2 mM. Excitation: 375 nm, emission: 440 nm, cut off at 420 nm. *T*=room temperature.

Interactions between ATMND ligand and hybrid DNA-RNA nanostructures were also tested in native PAGE experiments. Self-assembled hybrid RNA-DNA nanostructures, like 2-11 (**Figure 12**), can give rise to three well-defined and discrete bands (25) corresponding to triangle, square and pentagon, which had been demonstrated by another master student Alba Monferrer in our group. Presence of AP sites in 2-11 nanostructures would result in the bands running lower due to reduced mass (2-11-AP), however, ATMND labeled AP site-containing 2-11 nanostructures (2-11-AP-ATMND (10x), 2-11-AP-ATMND (20x)) would run higher than free-labeled AP site-containing 2-11 nanostructures, but lower (partly labeled) or similar (fully labeled) with standard 2-11 nanostructures without AP site (2-11). The gel is shown in **Figure 18a**. In order to amplify the amount of AP sites inserted by ATMND, ATMND was added 10 and 20 times over AP sites, but a band of 2-11-

AP-ATMND (10x) running to the same height with a band of 2-11-AP-ATMND (20x) implied that 10 times of ATMND over AP sites would be enough to result in distinct migration. And sample 2-11-ATMND (10x) and 2-11-ATMND (20x) indicated that ATMND ligand could not bind to nanostructures without AP site.

Alba Monferrer had also constructed a homogenous nanosquare, using a guide DNA oligomer which involved four DNA inner strands linked by particular linker sequences to build pure square nanoshapes (**Figure 18b**), which migrate slightly higher in a gel compared to the square band in the 2-11 mixture because the TU4-square contains more DNA nucleotides (25). This whole long DNA strand called TU4-miR can be found in **Table A1**. I built such TU4-square with DNA inner strand TU4-miR and complemented DNA out strand with AP site, where the target base opposite AP site was still cytosine. A titration gel with increased amounts of ATMND ligand was performed, using TU4-square containing AP site called TU4-AP (**Figure 18c**).

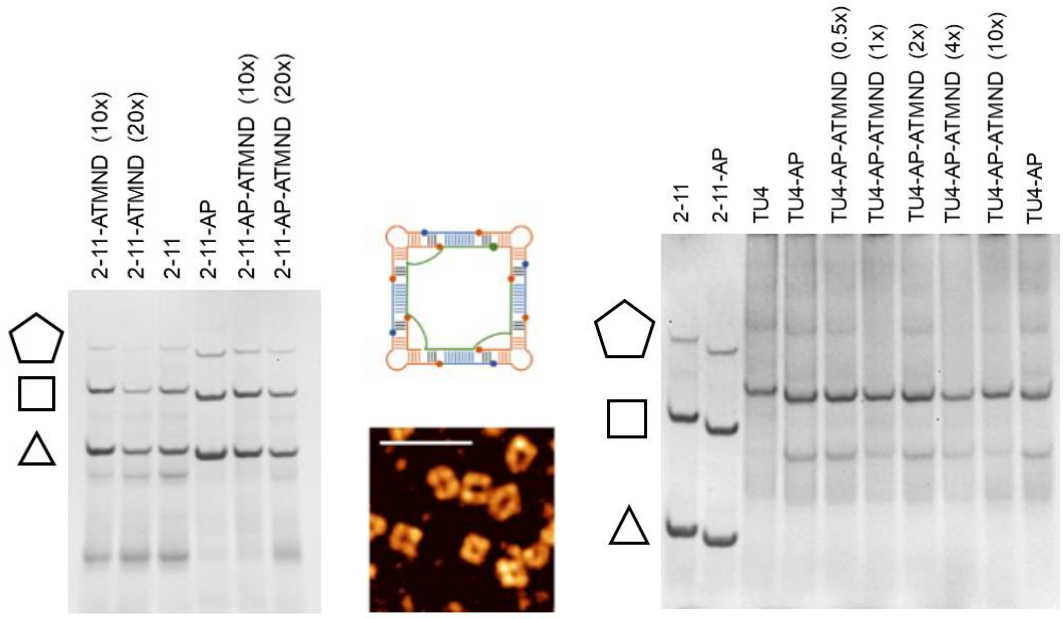

a **b** **c**

Figure 18. **a.** Interaction of ATMND ligand with AP site-containing 2-11 nanostructure (8% native PAGE containing 2 mM $MgCl_2$); **b.** Structure of TU4-square (25); **c.** Titration gel of ATMND over TU4-AP square (8% native PAGE containing 2 mM $MgCl_2$).

2. Design and synthesis of ATMND derivatives and studies of its affinity to AP site-containing DNA duplexes

2.1. ATMND derivatives design

Based on the good affinity and selectivity of ATMND to AP site opposite cytosine and thymine, we designed derivatives to introduce new chemical functionality to DNA containing abasic sites. In order to further functionalize ATMND, linkers were considered which are flexible to change length depending on the specific applications and endow ATMND with capacity to connect with other functional groups through covalent modification like click chemistry. Published studies about the structure-activity relationship of ATMND show that the three hydrogen bonds formation based on the 2-aminonaphthyridine frame toward the opposite nucleobases at neutral pH and the stacking interaction based on the

aromatic system with the nucleobases flanking the AP site (30) are responsible for its high affinity and selectivity (**Figure 19**), and the naphthyridine portion also plays the role of chromophore, absorbing UV and leading to the fluorescence behavior of ATMND.

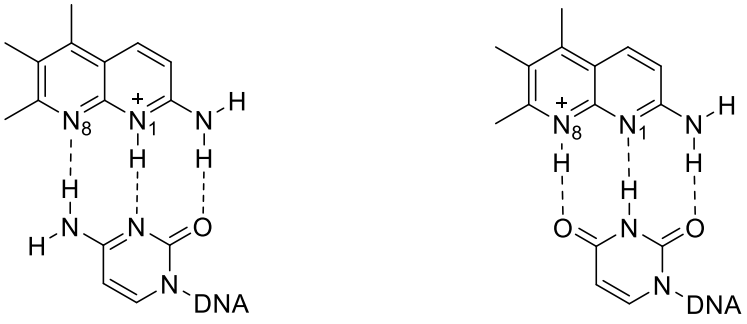

Figure 19. Proposed models of base-pairing between **a**. cytosine and N_1-protonated ATMND, **b**. thymine and N_8-protonated ATMND.

Apart from the main body, three methyl groups at C5, C6 and C7 are also reported contribute to the binding affinity of a series of 2-amino-1,8-naphthyridines molecules. Introduction of methyl groups attached to the naphthyridine ring effectively reduced the loss of binding entropy, resulting in the binding affinity clearly increasing for pyrimidine bases opposite the AP site in DNA duplexes according to a series of calorimetry experiments done by Sato and co-workers (17).

Considering the necessity to retain 2-amino-1,8-naphthyridine scaffold and the three methyl groups during modification, a linker was designed to add to the amino group by substituting a hydrogen atom (**Figure 20**).

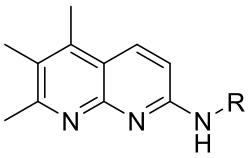

R= alkyl linker

Figure 20. Designed ATMND derivatives.

2.2. Alkyl-ATMND derivative synthesis and fluorescence studies

2.2.1. Alkyl-ATMND derivative synthesis

We first attempted to attach a hexyl group to ATMND as an alkyl linker. The ATMND halide **5** was deemed to be an essential intermediate to produce ATMND-linker derivatives from substitution with alkylamine. 2-Chloro-5,6,7-trimethyl-1,8-naphthyridine **5** was synthesized according to a literature procedure (31) (**Scheme 2**).

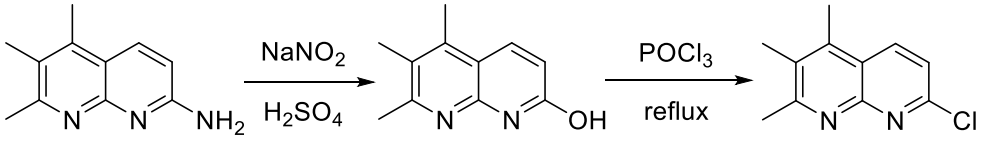

1 **4** **5**

Scheme 2. Synthesis of 2-chloro-5,6,7-trimethyl-1,8-naphthyridine **5**.

In this route, a diazotization reaction happened first with nitrous acid and sulfuric acid to activate the primary aromatic amine, giving the corresponding intermediate diazonium salt (**Figure 21**) while cooling on followed by a hydrolysis to give **4**. After that, halogenation was afforded in the presence of phosphoryl chloride at high temperature under argon gas protection to furnish **5**.

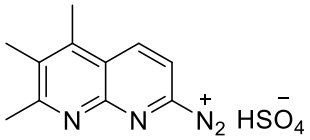

Figure 21. Diazonium salt intermediate to get compound **4**.

Nucleophilic aromatic substitution in the next step to give desired ATMND derivative **6** is relatively easy with a good yield around 80%. Chloride in compound **5** is a good leaving group at alpha position of nitrogen in the aromatic system and primary amine **7** serves as the nucleophile. Solvent is not needed in this reaction

system since hexan-1-amine is liquid in room temperature (**Scheme 3**).

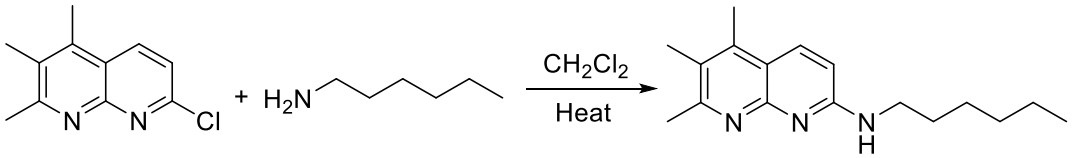

5 **7** **6**

Scheme 3. Synthesis of N-hexyl-5,6,7-trimethyl-1,8-naphthyridin-2-amine **6**.

2.2.2. Fluorescence studies about the interaction of Alkyl-ATMND derivative with AP site in DNA duplexes

The addition of an aminoalkyl side chain to ATMND was discussed by some groups. For instance, ATMND-3C-NH_2 was reported to have higher affinity to thymine through kinetic study (32) and ATMND-2C-NH_2 was proved to have increased affinity to adenine in A-site containing RNA (33). Although the linker I introduced was a simple alkyl chain, compound **6** was designed as a representative linker-extended 2-aminonaphthyridine DNA ligand, used to examine the capacity of linker-extended ATMND to bind to AP site contained in DNA duplexes. Fluorescence titration was done for 1 μM compound **6** in DMSO to 0 μM-10 μM 23-meric AP site-containing DNA duplexes (5'-CCT CGG ACG TG**X** CGA TA CGA GAC-3'/3'-GGA GCC TGC AC**N** GCT AT GCT CTG-5', **X**=AP site, **N**=T or C), in 10 mM sodium cacodylate buffer (pH 6.5) with 2 mM magnesium chloride at room temperature (**Figure 22**). All conditions were the same as the fluorescence titrations described for ATMND. The result indicates that alkyl extended ATMND still strongly (slightly stronger than ATMND) binds to cytosine opposite AP site at DNA duplexes, with an EC50 value of 0.37 μM. The titration of alkyl extended ATMND to thymine opposite AP site did not yield sigmoidal dose-response function.

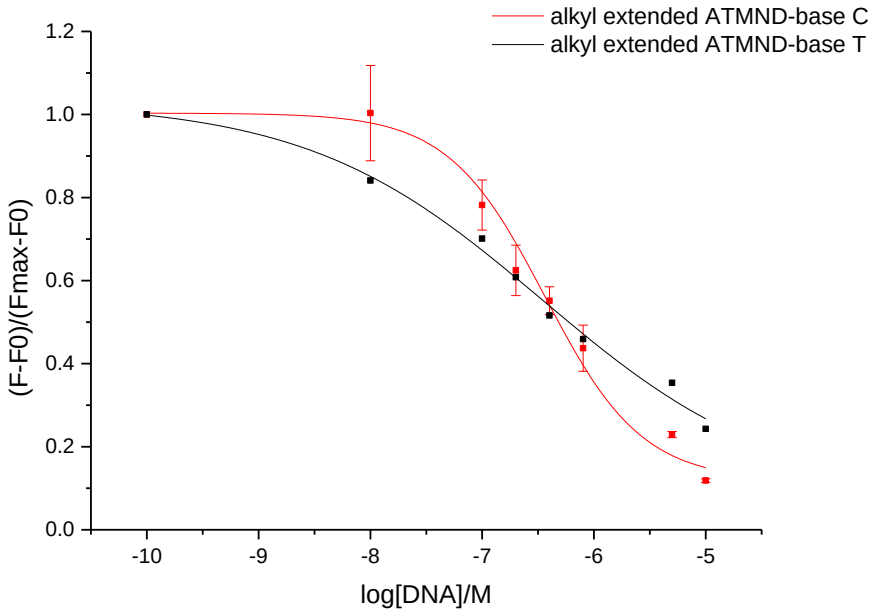

Figure 22. Fluorescence responses of **6** (1 μM) to target nucleobases (**N**=T(black), or C(red)) in 23-meric AP site-containing DNA duplexes in solutions buffered to pH 6.5 (10 mM sodium cacodylate) and containing $MgCl_2$ 2 mM. Excitation: 375 nm, emission: 440 nm, cut off at 420 nm. *T*=room temperature. Duplexes: 5'-CCT CGG ACG TG**X** CGA TA CGA GAC-3'/3'-GGA GCC TGC AC**N** GCT AT GCT CTG-5', **X**=AP site, **N**=T or C.

2.3. Alkyne-ATMND derivative synthesis and fluorescence studies

2.3.1. Alkyne-ATMND derivative synthesis

In order to functionalize the hybrid RNA-DNA nanostructure, an alkyne-ATMND derivative (**Figure 23**) was designed which has potential to incorporate any desired functional groups as azide derivatives through a click cycloaddition reaction.

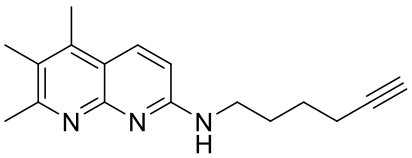

Figure 23. Designed alkyne-ATMND derivative.

In this synthesis pathway (**Scheme 4**), hex-5-yn-1-amine **8** had to be prepared first as the nucleophile to substitute the chloride of compound **5**. 6-

Phthalimido-1-hexyne **9** was obtained via reaction between 6-chloro-1-hexyne **10** and potassium phthalimide **11**, then followed by a stepwise cleavage of phthalimide moiety to obtain **8**. Hex-5-yn-1-amine is a volatile yellow oil synthesized through a route adapted from the literature (34).

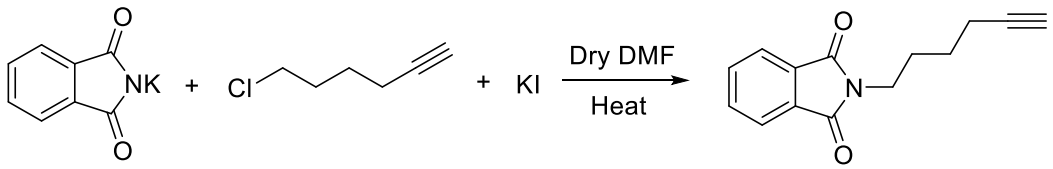

11 **10** **9**

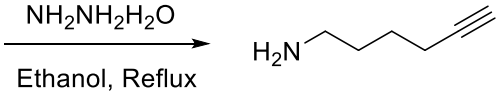

8

Scheme 4. Synthesis of hex-5-yn-1-amine **8**.

Thin-layer chromatography (TLC) was used with ninhydrin visualization of the amine product to monitor the progress of the reaction.

After hex-5-yn-1-amine **8** was obtained, S_N1 nucleophilic substitution with the ATMND halide gave N-(hex-5-yn-1-yl)-5,6,7-trimethyl-1,8-naphthyridin-2-amine **12** (**Scheme 5**). Compared with the similar substitution with hexan-1-amine, this reaction ran at a lower rate, more side product and lower yield (18%). Potassium carbonate was needed as a catalyst due to the poor reactivity of hexyn-1-amine. Purification was carried out by column chromatography on silica gel.

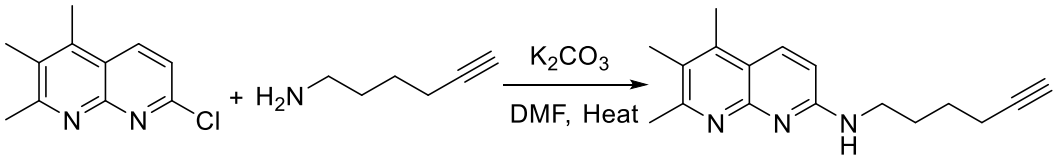

5 **8** **12**

Scheme 5. Synthesis of N-(hex-5-yn-1-yl)-5,6,7-trimethyl-1,8-naphthyridin-2-amine **12**.

3. Design and synthesis of ATMND-(6-TAMRA) conjugate and studies of its affinity to AP site-containing DNA duplexes and hybrid RNA-DNA nanostructures

3.1. Design of ATMND-(6-TAMRA) conjugate

Ratiometric fluorescent probes have been recognized as a promising fluorescence tool due to their high selectivity and precision. This technique uses two fluorescent molecules, records their fluorescence intensities at two different wavelengths and calculates the ratio (35). Fluorescence resonance energy transfer (FRET) is a mechanism describing energy transfer between two light-sensitive molecules. A donor chromophore, initially in its electronic excited state, may transfer energy to an acceptor chromophore through nonradiative dipole–dipole coupling. Based on FRET strategy, many different kinds of two-fluorophore hybrid probes have been applied, such as Alexa 488-Cy5 (36) and Cy3-Cy5 which was previously used by a PhD student in our group to monitor the formation of nanostructures.

In order to determine if the alkyne-ATMND derivative incorporated with a larger functional group can still bind to the AP site on DNA duplexes and hybrid RNA-DNA nanostructures constructed by our group, I designed a conjugated fluorophore

with ATMND and 6-TAMRA (6-carboxytetramethylrhodamine) (**Figure 24**), considering that the emission spectrometry of ATMND partly overlaps the excitation spectrometry of 6-TAMRA (**Figure 25**) so that FRET would happen with ATMND as energy donor and 6-TAMRA as acceptor.

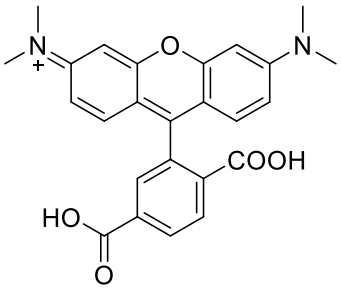

Figure 24. Structure of 6-TAMRA (6-carboxytetramethylrhodamine).

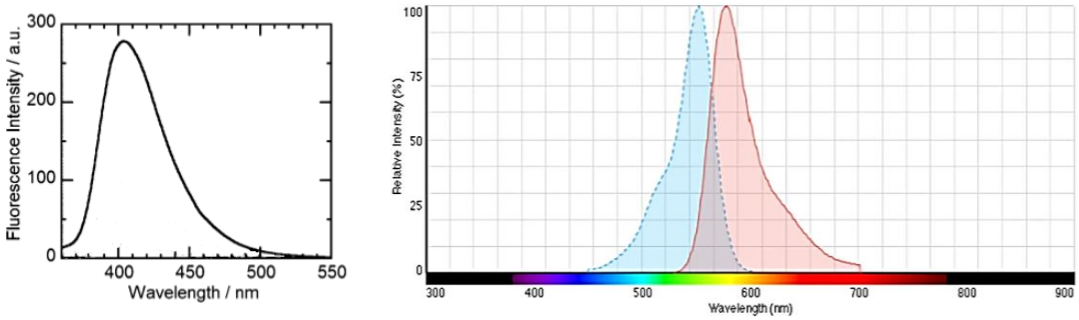

a **b**

Figure 25. Fluorescence spectrum of **a**. ATMND emission (26), **b**. 6-TAMRA.

3.2. Click chemistry and optimization of reaction conditions

A reasonable synthetic route to make a covalent dye-conjugated system containing rhodamine-based probe is click chemistry, forming a triazole linker through cycloaddition of alkyne-modified probe and azide group catalyzed by Cu (I) (**Figure 26**).

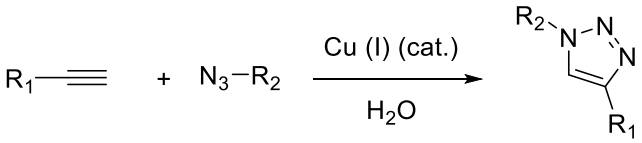

Figure 26. Click chemistry reaction.

Alkyne-modified ATMND **12** was obtained from as described above, and azide functionalized 6-TAMRA **13** is commercially available. A general procedure was implemented first with copper(II) sulfate served as catalyst, sodium ascorbic acid as reductant to reduce Cu (II) to Cu (I), triethylamine used to stabilize Cu (I)and methanol and water (1 : 1) as solvent, stirred at 60°C (37). While this attempt failed mass spectrometry analysis indicated the fragmentation of rhodamine framework since 6-TAMRA is unstable at high temperature (38). Although some copper-free click conditions have been published, like photo-click (39) for example, copper (I)-catalyzed azide/alkyne cycloaddition is still the most common way to produce 1,4-substituted triazoles. However, the reducing agents (like TCEP (40), DTT (41)), bases (like TBTA (42), DBCO-$PEG_4$5 (41)) and solvents (like DMF (43)) are also reported to apply. In order to seek accessible reaction conditions, (azidomethyl)benzene **14** was used to replace 6-TAMRA azide as a cheaper mock azide probe in the click reaction with alkyne-ATMND derivative **12** (**Scheme 6**) and different conditions (**Table 1**) were explored. Finally, a most feasible condition concluding reducing agent sodium ascorbic acid, catalyst-base copper (II)-TBTA and solvent methanol and water (1:1) was found to make sure the aimed product obtained at room temperature during a relatively short time.

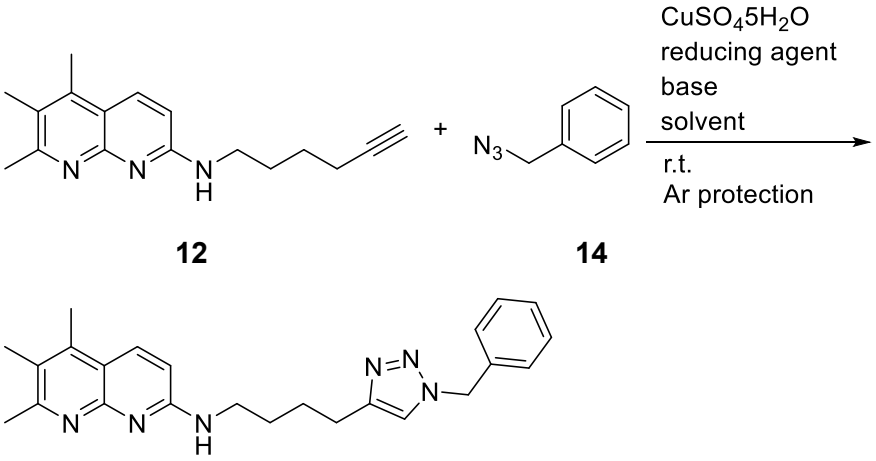

12 **14**

15

Scheme 6. N-(4-(1-benzyl-1H-1,2,3-triazol-4-yl)butyl)-5,6,7-trimethyl-1,8-naphthyridin-2-amine **15**

Table 1. Different conditions attempted for click chemistry reaction.

Group	Reducing agent	Base	Solvent
1	ascorbate	Et_3N	DMF : H_2O=1 : 1
2	ascorbate	Et_3N	Methanol : H_2O=1 : 1
3	TCEP	TBTA	DMF : H_2O=1 : 1
4	TCEP	TBTA	Methanol : H_2O=1 : 1
5	ascorbate	TBTA	DMF : H_2O=1 : 1
6	ascorbate	TBTA	Methanol : H_2O=1 : 1
7	ascorbate	TBTA	Methanol : H_2O=4 : 1

3.3. Synthesis of ATMND-(6-TAMRA) conjugate

Copper (II)-TBTA complex proved an effective component used for click chemistry reaction. Although 10 mM copper (II)-TBTA in 55% aq. DMSO is commercially available, considering the high boiling point of water and DMSO,

copper (II)-TBTA in 100% MeOH was made for substitution. The mixture of $CuSO_4 5H_2O$ (0.025 g, 0.10 mmol) and TBTA (0.058 g, 0.26 mmol) were dissolved in 10 ml methanol to give 10 mM copper (II)-TBTA in 100% MeOH as blue solution The structure of TBTA (Tris((1-benzyl-4-triazolyl)methyl)amine) shows below (**Figure 27**).

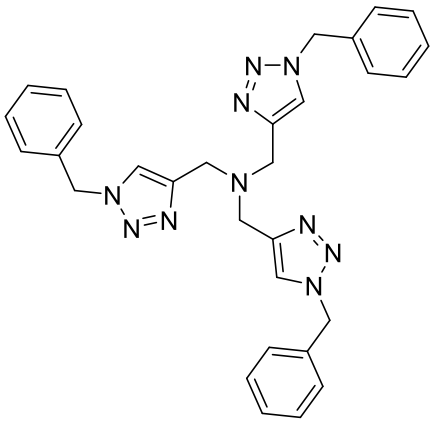

Figure 27. Structure of TBTA (Tris((1-benzyl-4-triazolyl)methyl)amine).

Due to the limited amount of available 6-TAMRA azide, this reaction was done at a microscale. All materials were prepared as solutions and were reacted in Eppendorf tubes for 2 to 3 days. Since it is difficult to remove all oxygen from an Eppendorf tube, reducing agent and catalyst were replenished several times during the whole reaction process to ensure that sufficient Cu (I) was available. Since 6-TAMRA is sensitive to visible light (380nm-780nm) and can be excited in this wavelength range, this reaction was performed in the dark to avoid exposure to light. The final product ATMND-(6-TAMRA) **16** was stable at room temperature and separated from TLC plate. (**Scheme 7**)

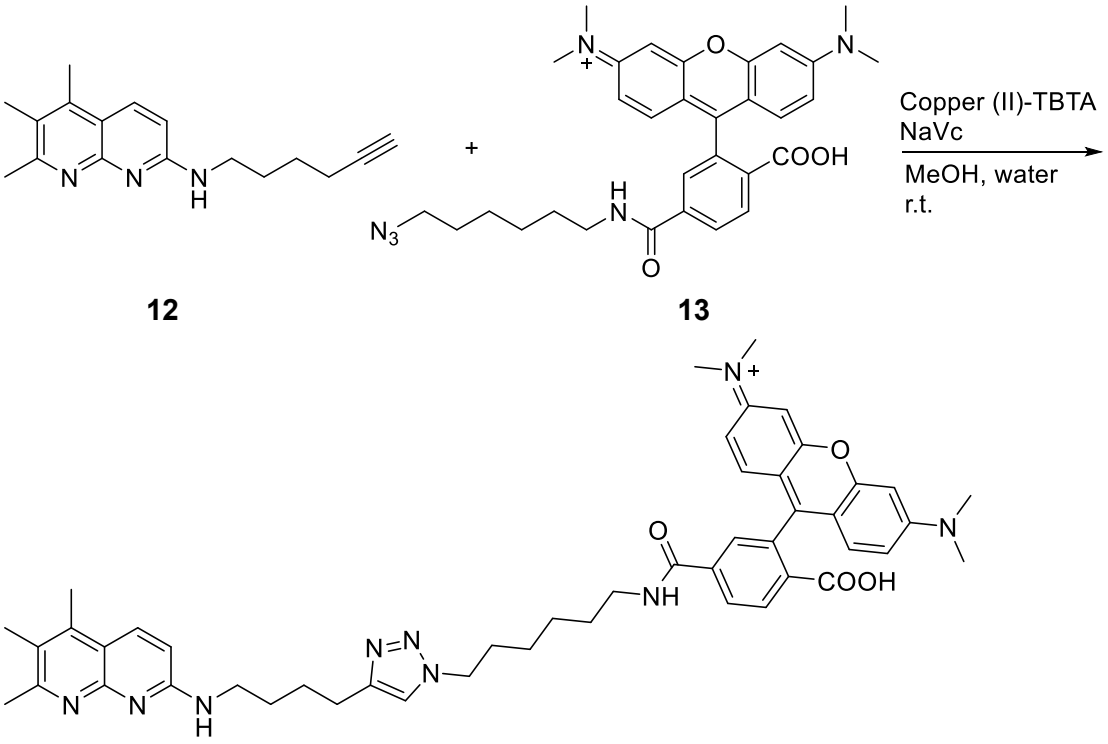

12 **13**

16

Scheme 7. Synthesis of ATMND-(6-TAMRA) **16**.

3.4. Fluorescence studies of the interaction of ATMND-(6-TAMRA) with AP site-containing DNA duplexes

3.4.1. Concentration verification of ATMND-(6-TAMRA)

In the synthesis process of ATMND-(6-TAMRA), I found that this compound was unstable in the rotary evaporator. Therefore, its solution in methanol obtained from TLC plates was concentrated at normal pressure and temperature, and then dissolved in DMSO, stored in -20°C freezer for further testing. In order to verify the real concentration of this ATMND-(6-TAMRA) solution, a standard curve method was used. 6-TAMRA solid at an accurately determined weight was dissolved in and diluted by DMSO to construct a dilution series. Fluorescence intensities were measured with increased concentrations of 6-TAMRA. Data for known concentrations of 6-TAMRA were used to prepare a standard curve, with

concentration on X axis and fluorescence intensity on Y axis (**Figure 28**); the R-square of a linear fit was 0.9997. The same assay was also performed with a sample of ATMND-(6-TAMRA) and its concentration was calculated based on the standard curve.

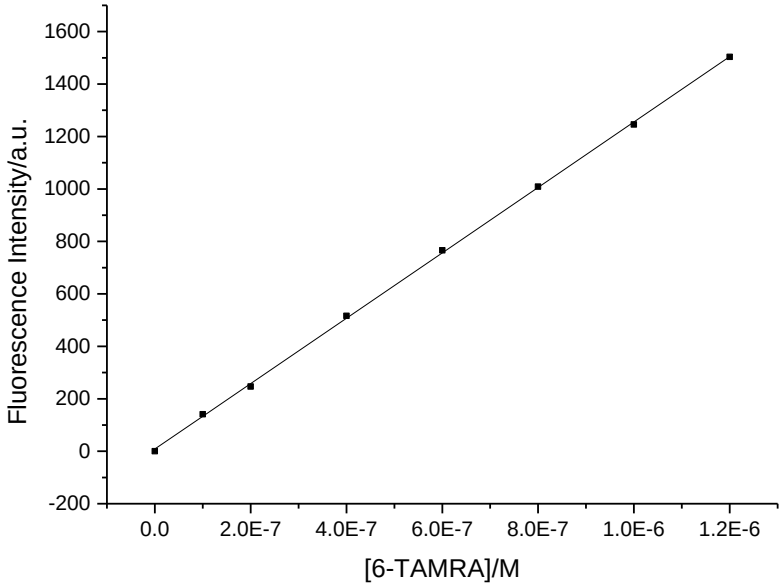

Figure 28. Standard curve of 6-TAMRA, measured in solution buffered to pH 6.5 (10 mM sodium cacodylate) containing 2 mM $MgCl_2$ at room temperature. Excitation: 543 nm. Emission: 610 nm.

3.4.2. FRET Study of ATMND-(6-TAMRA) dye-conjugate

The distance at which the energy transfer is 50% efficient is defined as Förster distance, which can be 2 nm to 10 nm for commonly used fluorophores. The length of the linker between ATMND (donor) moiety and 6-TAMRA (acceptor) moiety of compound **16** is slightly more than 2 nm, placed within effective distance. Thus, the fluorescence spectra of ATMND and ATMND-(6-TAMRA) were measured (**Figure 29**). Concentrations of both compounds were 0.25 μM. ATMND was excited at 375 nm, range of emission wavelength detected was from 400 nm to 700 nm, and a clear

ratiometric response was obtained based on quenching of ATMND emission (430 nm) and enhancing of 6-TAMRA emission (580 nm).

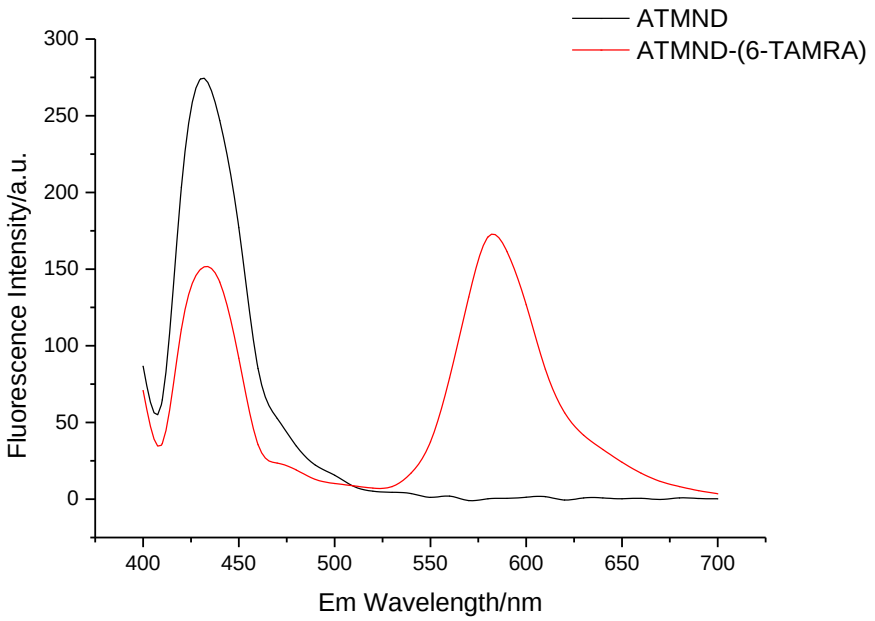

Figure 29. Fluorescence spectra of ATMND (0.25 μM, black) and ATMND-(6-TAMRA) (0.25 μM, red), measured in solution buffered to pH 6.5 (10 mM sodium cacodylate) containing 2 mM $MgCl_2$ at room temperature. Excitation: 375 nm.

3.4.3. Fluorescence studies of ATMND-(6-TAMRA) binding to AP site-containing DNA duplexes

Fluorescence responses of ATMND-(6-TAMRA) were measured by titration experiments upon addition of 23-meric AP site-containing DNA duplexes (5'-CCT CGG ACG TG**X** CGA TA CGA GAC-3'/3'-GGA GCC TGC AC**N** GCT AT GCT CTG-5', **X**=AP site, **N**=T or C) at room temperature in solution buffered to pH 6.5 (10 mM sodium cacodylate) with 2 mM magnesium chloride. The ATMND moiety exhibited emission quenching with increasing concentration of DNA duplexes (**Figure 30**). However, the binding affinity of compound ATMND-(6-TAMRA) was observed lower than that of ATMND, at an EC50 value of 3.11 μM.

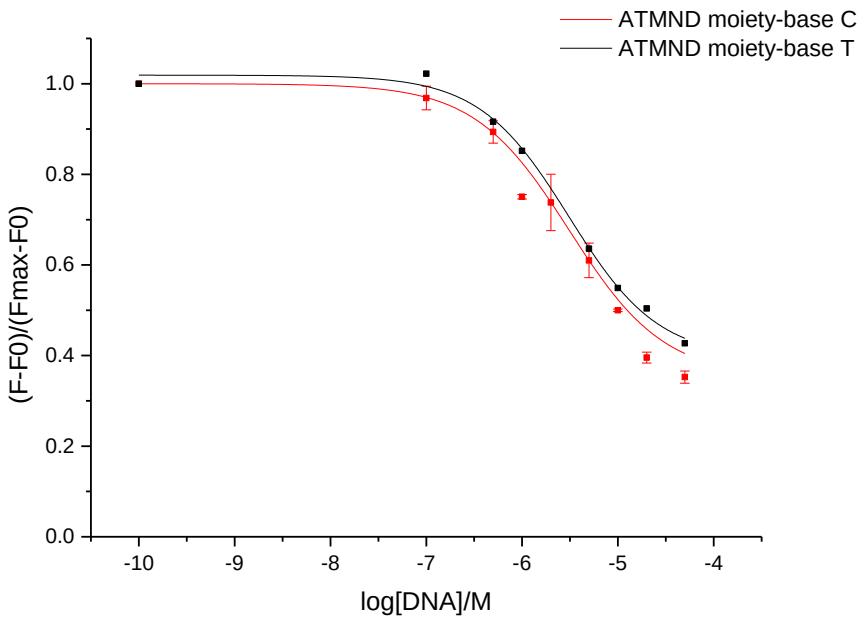

a

Figure 30. Fluorescence responses of ATMND moiety in ATMND-(6-TAMRA) (1.0 μM) binding to cytosine (red, N=C) and thymine (black, N=T) in the 23-meric AP site-containing DNA duplexes in solution buffered to pH 6.5 (10 mM sodium cacodylate) with 2 mM magnesium chloride. Excitation: 375 nm. Emission: 440 nm.

Various reasons have been mentioned to influence binding affinity and selectivity of dye-conjugated AP site ligands, for example, the length of linker between two units (44), and I conjectured that the reason may also lie in steric hindrance caused by the large moiety of 6-TAMRA. The fluorescence of 6-TAMRA moiety was found to remain nearly unchanged when adding DNA duplexes, neither quenching nor enhancement, which suggested that no observable interaction between 6-TAMRA moiety and AP site-containing DNA duplexes occurred (**Figure 31**).

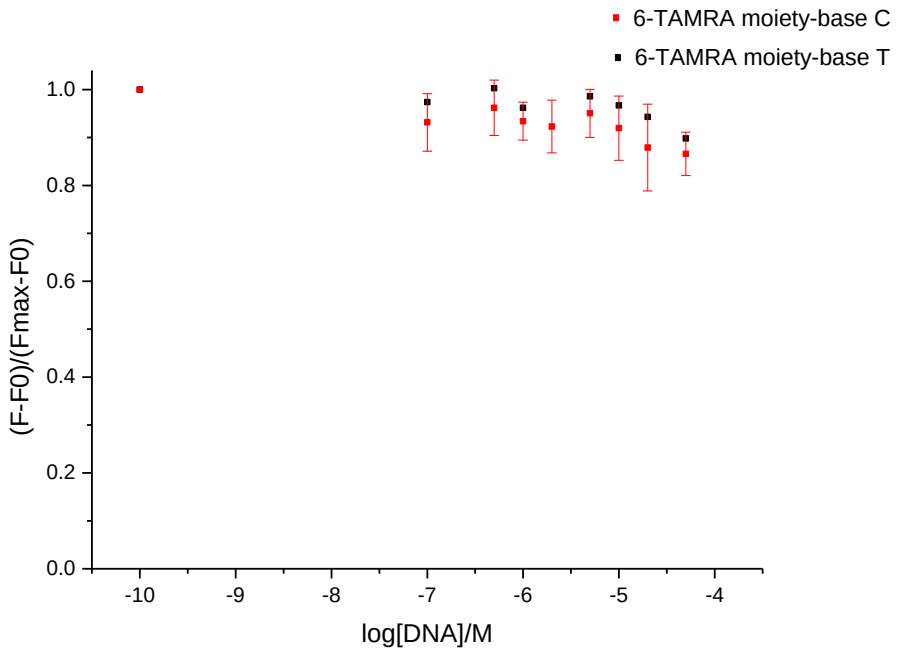

b

Figure 31. Fluorescence responses of 6-TAMRA moiety in ATMND-(6-TAMRA) (1.0 μM) binding to cytosine (red, N=C) and thymine (black, N=T) in the 23-meric AP site-containing DNA duplexes in solution buffered to pH 6.5 (10 mM sodium cacodylate) with 2 mM magnesium chloride. Excitation: 543 nm. Emission: 610 nm.

And the FRET manifested moderately decreasing which resulted from more energy of excited ATMND moiety dissipated through static quenching, stacked by both flanking nucleobases, while less left through FRET and light emission (**Figure 32**).

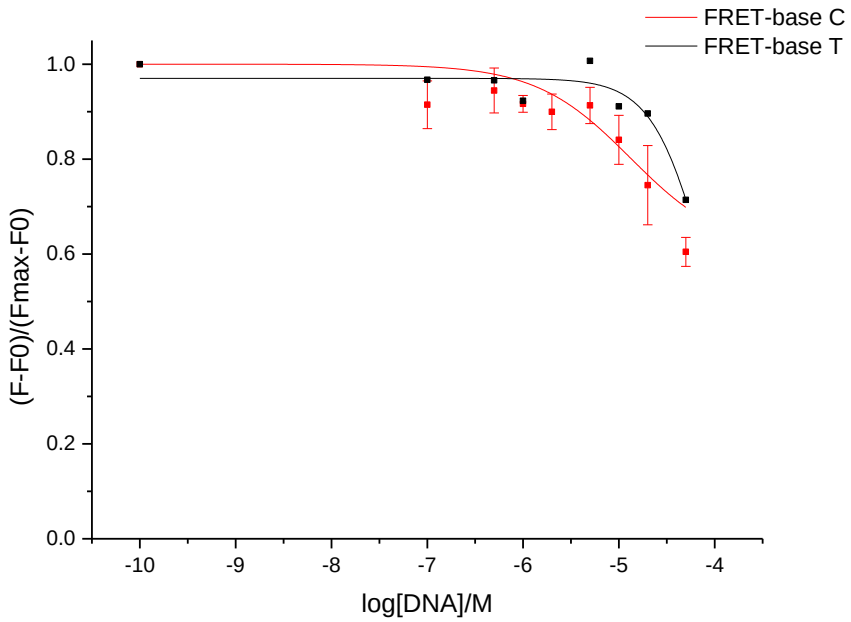

c

Figure 32. Fluorescence responses of FRET in ATMND-(6-TAMRA) (1.0 μM) binding to cytosine (red, N=C) and thymine (black, N=T) in the 23-meric AP site-containing DNA duplexes in solution buffered to pH 6.5 (10 mM sodium cacodylate) with 2 mM magnesium chloride. Excitation: 375 nm. Emission: 610 nm.

3.5. Fluorescence studies of the interaction of ATMND-(6-TAMRA) with AP site-containing hybrid RNA-DNA nanostructures

3.5.1. Double-FRET probes design

6-TAMRA and Cy5 have been reported to be developed as FRET probes for protein studies (45), in which 6-TAMRA served as FRET donor and Cy5 served as FRET acceptor. Simultaneously, the fluorescence of donor ATMND could also be quenched by 6-TAMRA as acceptor due to FRET. Based on both facts, I designed a strategy to study affinity of ATMND-(6-TAMRA) to AP site on hybrid nanostructures.

A PhD student in our group had designed a corner RNA module strand conjugated with a 5'-termonal Cy5 (46). The base sequences and position of dye Cy5 are shown in **Figure 32a**. Once ATMND moiety of synthesized dye conjugate

ATMND-(6-TAMRA) binds to AP site through hydrogen bonds, fluorescence resonance energy would transfer from ATMND moiety to 6-TAMRA moiety, and then from 6-TAMRA moiety to Cy5 fixed on RNA corner, double FRET would happen synergistically, as shown in **Figure 32b**.

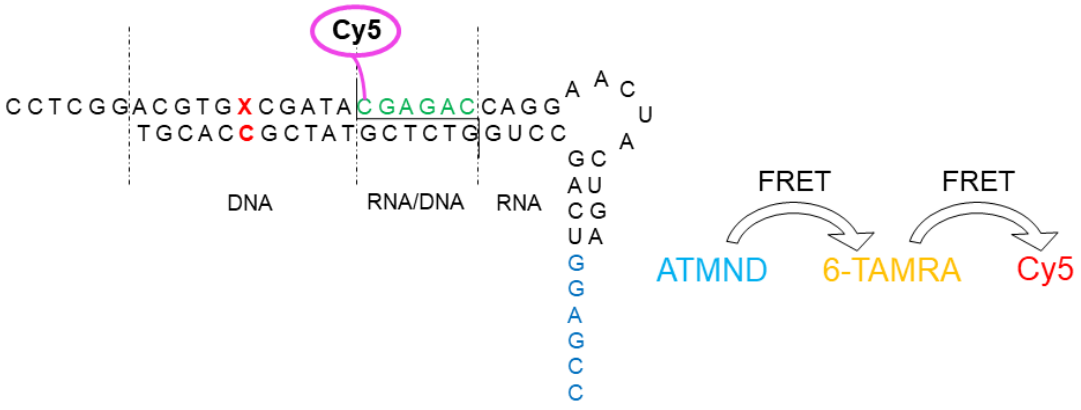

a **b**

Figure 33. **a**. Repeating segment of 2-11 nanostructures connected with dye Cy5, **b**. Double FRET strategy.

A fluorescence titration was done via increasing concentration of AP site at 2-11 hybrid RNA-DNA nanostructures and keeping constant concentration of ATMND-(6-TAMRA) and Cy5. In this concept, each sample for testing would have same total amount of nanostructures (1 μM) and ligand (1 μM), while changed ratio of DNA modules with AP site to those without AP site (0:1, 1:2, 1:1, 2:1, 1:0) forming the nanoshapes. All samples were dissolved in 10 mM HEPES buffer (pH 7) including 2 mM magnesium chloride. The fluorescence intensities are shown in **Figure 33**. Unfortunately, neither excited ATMND (**Figure 33a**) nor excited 6-TAMRA (**Figure 33b**) transferred energy to Cy5 moiety (emission of Cy5 was expected to appear at around 680 nm) with increasing proportion of AP site, which indicated weak or no effective binding of ATMND-(6-TAMRA) to AP site-containing nanostructures.

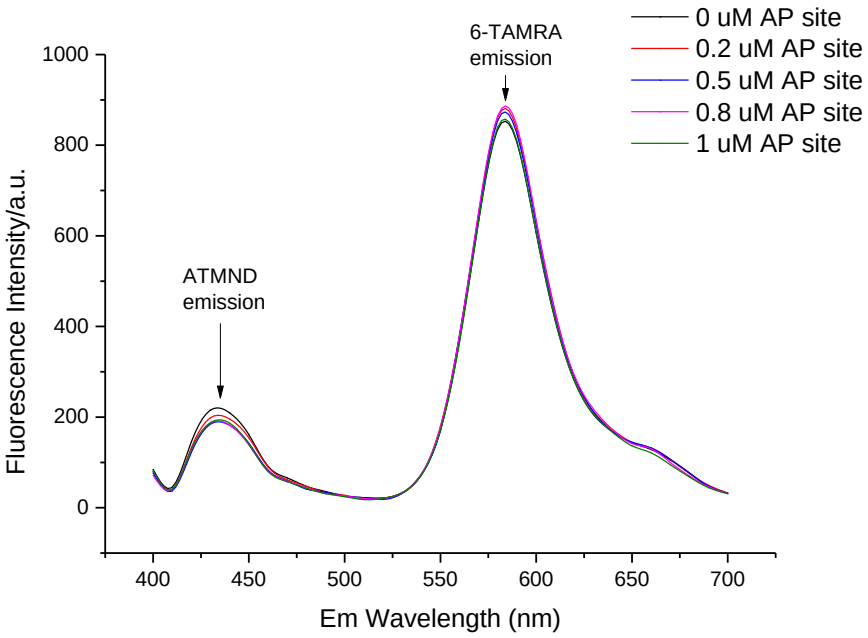

a

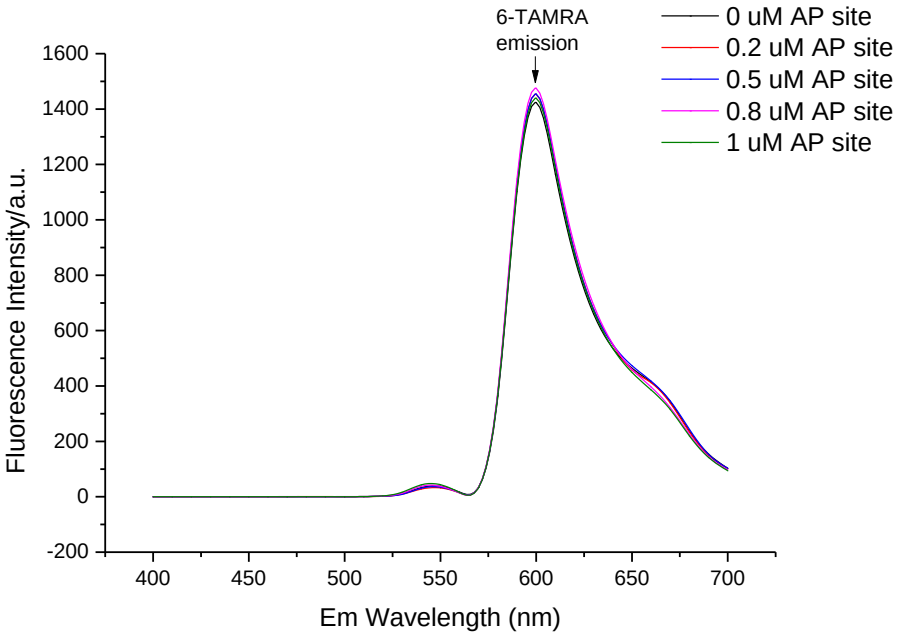

b

Figure 34. Fluorescence spectra changes of ATMND-(6-TAMRA) (1 μM) to target nucleobase cytosine opposite AP site contained in 2-11 nanostructures and Cy5 (1 μM) connected to corner RNA out strand with increasing proportion of AP site (**a.** excited ATMND moiety at 375 nm, **b.** excited 6-TAMRA moiety at 543 nm).

Since the results of FRET assay proved difficult to further study the affinity of my dye conjugate ATMND-(6-TAMRA) to AP site-containing 2-11 nanostructures, I

tried to run a native PAGE gel to explore the reasons for the low binding affinity. I supposed that the reason lies in either the three hydrogen bonds formed by ATMND moiety not strong enough to bind to AP site on nanostructures with a burden of such a large molecule, or 6-TAMRA interfering formation of our hybrid nanoshapes, or both. Therefore, linker-extended ATMND (compound **6**), 6-TAMRA and ATMND-(6-TAMRA) were separately added into AP site-containing 2-11 nano samples. The gel is shown in **Figure 34**. Based on this gel, 6-TAMRA would not interfere the formation of our hybrid RNA-DNA nanostructures, and similar with ATMND-(6-TAMRA), linker-extended ATMND was unable to bind to AP site on the nanostructures as well. So, I believe that three hydrogen bonds formed between ATMND moiety and cytosine opposite AP site are not strong enough to support ATMND connected with a linker chain tightly binds to AP sites of nanostructures.

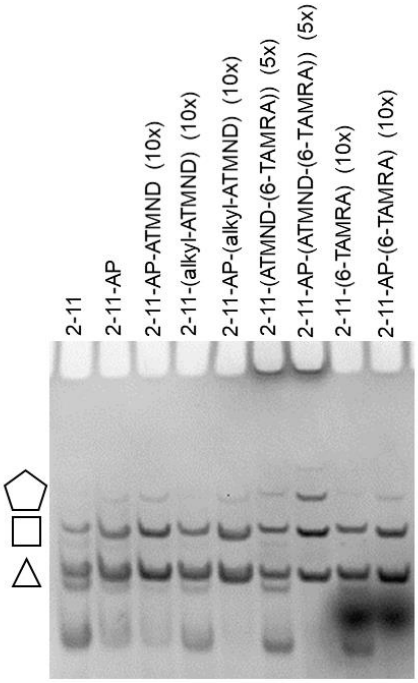

Figure 35. Interaction of AP site-containing 2-11 nanostructures with ATMND, linker-extended ATMND, ATMND-(6-TAMRA) and 6-TAMRA (5% native PAGE containing 2 mM $MgCl_2$).

4. Design and synthesis of an ATMND dimer

4.1. Synthesis of an ATMND dimer

Considering the strong affinity and selectivity of ATMND to AP site opposite cytosine and thymine of DNA duplexes and poor binding to AP site-containing hybrid RNA-DNA nanostructures, I designed an ATMND dimer, in which two ATMND moieties on both ends of a long enough linker serve as AP site binding ligands to potentially connect between two AP sites on one hybrid RNA-DNA nanostructure with its both ATMND moieties. This approach may be a method to strengthen the interaction between ligands and AP sites on nano frameworks or to generate hydrophobic cavities within RNA-DNA hybrid nanostructures. The ATMND dimer also has the potential to connect two or more nanostructures with AP sites together to build more complex nano architectures from RNA-DNA hybrids.

The first step was synthesis of N^1,N^{12}-bis(5,6,7,-trimethyl-1,8-naphthyridin-2-yl)dodecane-1,12-diamine **17** through S_N1 nucleophilic substitution with ATMND halide **5** of amino groups on both ends of 1,12-diaminedodecane. (**Scheme 8**)

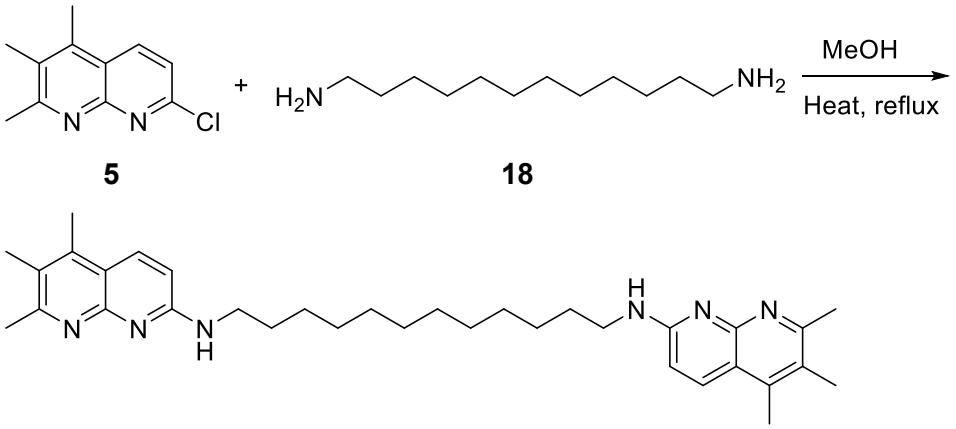

5 **18**

17

Scheme 8. Synthesis of ATMND dimer **17.**

4.2. Interaction study of ATMND dimer with AP site-containing RNA-DNA hybrid nanostructures

A native PAGE experiment was performed to investigate the interaction between ATMND dimer **17** with our hybrid nanoshapes containing AP site opposite cytosine and to compared to binding of ATMND monomer. The gel is shown in **Figure 35**. From this gel, it is appears that AP site-containing nanoshapes in the presence of ATMND dimer moved slower than ligand free nanostructures with AP site. Higher complexes involving more than one nanostructure were not observed on this gel, which indicates that ATMND dimer bonded with two AP sites within the same nanostructure. ATMND dimer, as a promising ligand to functionalize the hybrid nanostructures developed in our lab, has a potential to form six hydrogen bonds with two cytosines opposite AP sites simultaneously with both ATMND moieties, which strengthens the binding interaction between ligands and nanostructures. Further studies of ATMND dimer planned.

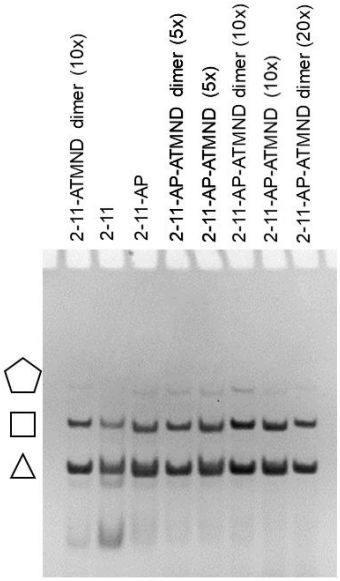

Figure 36. Interaction of AP site-containing hybrid RNA-DNA nanostructures with ATMND dimer (5% native PAGE containing 2 mM $MgCl_2$).

5. Summary

In this project, ATMND was demonstrated to serve as a useful ligand to non-covalently decorate hybrid RNA-DNA nanostructures containing AP sites. Although linker-extended ATMND derivative showed a weak interaction with AP site-containing nanoshapes, an ATMND dimer managed to strengthen ligand-abasic site binding on RNA-DNA hybrid nanoshapes and may have a potential to connect multiple nanoshapes to build complex nano-architectures.

In future research, other different types of functional molecules may be added to hybrid RNA-DNA nanostructures by using ATMND as a targeting ligand. Additional experiments with the ATMND dimer should be conducted to functionalize hybrid nanostructures and construct complex nucleic acidic nanoparticles.

Materials and methods

1. General information

Commercial reagents and anhydrous solvents were purchased from standard suppliers and used without further purification. 6-TAMRA azide was purchased from Biotium. The progress of reactions was monitored by TLC pre-coated silica gel G plates. TLC plates were visualized in UV light or staining with ninhydrin solution (compound **7** and **8**). Column chromatography was carried out to purify desired products with silica gel. ^{1}H-NMR spectra were recorded using Burker AVA machine (operating at 300 Hz for ^{1}H-NMR and 500 Hz for ^{13}C-NMR) relatively using chloroform-d4 or Methanol-d4 as solvent. ^{1}H-NMR spectra were internally referenced to 7.26 ppm for chloroform-d4 and 3.31 ppm for methanol-d4. Mass characterization was performed by mass spectrometry facility of the Department of Chemistry and Biochemistry at UC San Diego.

All RNA and DNA oligonucleotides were purchased from Integrated DNA Technologies at 100 nmole synthesis scale with desalting, HPLC, or PAGE purification. RNA and DNA stock solution were prepared by dissolving lyophilized single stranded oligonucleotides in 10 mM sodium cacodylate solution buffered pH 6.5. The concentrations of RNA and DNA stock solution were verified with UV-Vis recording Shimadzu spectrophotometer (UV-2401PC) in a 1 cm x 1 cm quartz cuvette, measured absorptions at 260 nm.

2. Compounds synthesis

2.1. Synthesis of 2-amino-5,6,7-trimethyl-1,8-naphthyridin (ATMND) 1

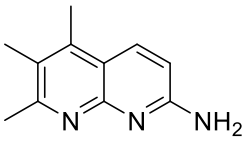

Figure 37. Structure of 2-amino-5,6,7-trimethyl-1,8-naphthyridin (ATMND) **1**.

2,6-Diaminopyridine **2** (2.00 g, 18.33 mmol) and 3-methylpentane-2.4-dione **3** (2.20 g, 19.24 mmol) were mixed in phosphoric acid (85%, 50 ml), the solution was stirred for 24 hours at 95°C and cooled down to room temperature. The reaction mixer was neutralized with 1 M aqueous NaOH and then filtered to remove salt. The residue was extracted with chloroform three times and combined organic phase was dried over anhydrous sodium sulfate and concentrated under reduced pressure to get brown solid. The crude product was purified by silica column chromatography (DCM: MeOH=15:1) to give pure desired product **1** as shallow brown solid powder (0.92 g, 4.91 mmol, 41% yield). ^{1}H-NMR (300 MHz, Methanol-d4): 8.12 (d, 1H, *J*=9.1 Hz), 6.80 (d, 1H, *J*=9.1 Hz), 2.58 (s, 3H), 2.51 (s, 3H), 2.31 (s, 3H). LR-MS ([M+H]$^{+}$): 188.32.

2.2. Synthesis of 2-chloro-5,6,7-trimethyl-1,8-naphthyridine 5

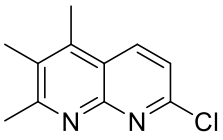

Figure 38. Structure of 2-chloro-5,6,7-trimethyl-1,8-naphthyridine **5**.

Sodium nitrite (0.38 g, 5.51 mmol) dissolved in 4 ml water was added to a mixture of ATMND **1** (0.50 g, 2.67 mmol) in 47% H_2SO_4 10 ml at ice bath. The reaction solution was stirred at 0 °C for 4 hours and then at 90°C for another 4 hours. The clear yellow reaction solution was cooled down to room temperature and was stirred for anoth8r 2 hours, followed by neutralization with ammonia monohydrate

and made slightly basic. After filtration, the filtrate was extracted with chloroform five times. The organic solution was dried over anhydrous sodium sulfate and concentrated in vacuo to give 2-hydroxyl-5,6,7-trimethyl-1,8-naphthyridine as a pale-yellow powder **4** (0.32 g, 1.70 mmol, 64% yield).

Crude product **4** (0.30 g, 1.59 mmol) was moved into a two-neck flask, mixed with 1.3 ml phosphoryl chloride. The reaction mixture was stirred and refluxed at 130°C under argon gas protection for 3 hours. The deep violet solution was cooled down to room temperature, then neutralized with ammonia monohydrate to pH 8 and extracted with chloroform 3 times. The combined organic layer was washed with brine and dried over anhydrous sodium sulfate. All solvent was evaporated under reduced pressure to give 2-chloro-5,6,7-trimethyl-1,8-naphthyridine **5** as a pale yellow solid (0.30 g, 1.46 mmol, 91% yield) (**Figure 36**). ^{1}H-NMR (300MHz, Methanol-d4): 8.83 (d, 1H, *J*=7.0 Hz), 7.85 (d, 1H, *J*=8.9 Hz), 2.91 (s, 3H), 2.87 (s, 3H), 2.55 (s, 3H). LR-MS ([M+H]$^{+}$): 207.27.

2.3. Synthesis of N-hexyl-5,6,7-trimethyl-1,8-naphthyridin-2-amine 6

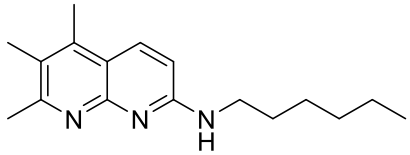

Figure 39. Structure of N-hexyl-5,6,7-trimethyl-1,8-naphthyridin-2-amine **6**.

To a solution of 2-chloro-5,6,7-trimethyl-1,8-naphthyridine **5** (0.10 g, 0.48 mmol) dissolved in 2 ml dichloromethane, hexan-1-amine **7** (0.6 ml, 5 mmol) was added. The reaction solution was stirred at 80°C for 4 hours. After cooled down to room temperature, the mixture was extracted with dichloromethane three times, the

organic phase was washed with 1 M NaOH and dried over anhydrous sodium sulfate. The solvent was concentrated under reduced pressure to give N-hexyl-5,6,7-trimethyl-1,8-naphthyridin-2-amine as brown gum (0.10 g, 0.37 mmol, 77% yield). ^{1}H-NMR (300MHz, Methanol-d4): 8.02 (d, 1H, *J*=9.1 Hz), 6.72 (d, 1H, *J*=9.2 Hz), 4.13 (s, 1H), 3.49 (t, 2H, *J* = 7.1 Hz), 2.57 (s, 3H), 2.50 (s, 3H), 2.31 (s, 3H), 1.64 (dd, *J* = 13.5, 6.3 Hz, 2H), 0.90 (s, 9H). HR-MS (ESI) for $C_{17}H_{25}N_3$ ($[M+H]^+$): 272.2122.

2.4. Synthesis of 6-phthalimido-1-hexyne 9

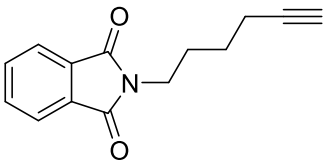

Figure 40. Structure of 6-phthalimido-1-hexyne **9**.

A round-bottom flask was charged with potassium phthalimide **11** (0.95 g, 5.16 mmol) and potassium iodide (0.71 g, 4.30 mmol) dissolved in 17 ml anhydrous DMF. 6-Chloro-1-hexyne **10** (0.48 ml, 4.29 mmol) was added to give yellow suspension. The reaction mixture was stirred at 80°C for 20 hours under argon gas protection to get transparent yellow solution. After being cooled down to room temperature, the resulting solution was added 20 ml water and then the product was extracted with diethyl ether 4 times. The organic phases were combined and dried over anhydrous sodium sulfate. The solvent was concentrated in rotary evaporator to give a white solid. This crude product was purified via silica column chromatography to get pure 6-phthalimido-1-hexyne **9** as white crystalline solid (0.65 g, 2.88 mmol, 67% yield). ^{1}H-NMR (300MHz, $CDCl_3$): 7.92 – 7.79 (m, 2H), 7.70 (m, 2H), 3.69 (t, *J* = 7.1 Hz, 2H), 2.23 (td, *J* = 7.0, 2.6 Hz, 2H), 1.92 (t, *J* = 2.6 Hz, 1H),

1.87 – 1.72 (m, 2H), 1.65 – 1.48 (m, 4H). LR-MS ([M+H]$^+$): 228.23.

2.5. Synthesis of Hex-5-yn-1-amine 8

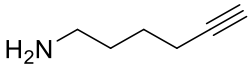

Figure 41. Structure of hex-5-yn-1-amine **8**.

Hydrazine hydrate (2.09 ml, 43.00 mmol) was added to a white suspension of 6-phthalimido-1-hexyne **9** (1.95 g, 8.60 mmol) in 17 ml ethanol. The reaction mixture was refluxed at 80°C for 2 hours. At first, the white suspension dissolved resulting into a transparent solution, and then a large amount of white precipitate appeared. The reaction mixture was cooled down to room temperature and 10 ml water was added to dissolve all precipitate. Enough diethyl ether was added until no more white solid arose. The white solid was filtered out and washed with diethyl ether five times and the aqueous layer was further extracted with diethyl ether for five times as well. All diethyl ether portions were combined, washed with brine and dried over anhydrous sodium sulfate. Solvent was removed on a rotary evaporator to give hex-5-yn-1-amine **8** as a pale-yellow oil residue (0.40 g, 4.15 mmol, 48% yield). ^{1}H-NMR (300MHz, $CDCl_3$): 4.71 (s, 2H), 2.66 (s, 2H), 2.16 (d, *J* = 2.5 Hz, 2H), 2.12 (d, *J* = 1.1 Hz, 2H), 1.90 (t, *J* = 2.6 Hz, 1H), 1.73 (d, 2H). LR-MS ([M+H]$^+$): 98.03.

2.6. Synthesis of N-(hex-5-yn-1-yl)-5,6,7-trimethyl-1,8-naphthyridin-2-amine 12

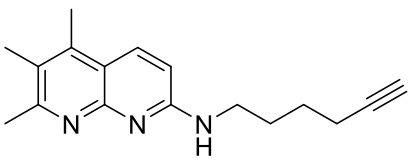

Figure 42. Structure of N-(hex-5-yn-1-yl)-5,6,7-trimethyl-1,8-naphthyridin-2-amine **12**.

A two-neck flask was charged with a mixture of 2-chloro-5,6,7-trimethyl-1,8-naphthyridine **5** (0.10 g, 0.48 mmol) and potassium carbonate (0.10 g, 0.72 mmol), hex-5-yn-1-amine **8** (0.40 g, 4.12 mmol) dissolved in 2 ml DMF was added. The reaction mixture was connected to condensate water because hex-5-yn-1-amine is volatile, stirred at 80°C for 20 hours. After cooling down to room temperature and extraction with dichloromethane for 4 times, the organic layers were combined, washed with 1 M NaOH and brine and then dried over anhydrous sodium sulfate. The solvent was removed under reduced pressure. The residue was purified through silica column chromatography (ethyl acetate : methanol = 25 : 1), and n-(hex-5-yn-1-yl)-5,6,7-trimethyl-1,8-naphthyridin-2-amine **12** was isolated as red oil (0.02 g, 0.08 mmol, 17% yield). ^{1}H-NMR (300MHz, $CDCl_3$): 8.05 (d, *J* = 9.2 Hz, 1H), 6.79 – 6.69 (d, 1H), 5.11 (s, 1H), 3.54 (t, *J* = 7.2 Hz, 2H), 2.69 (s, 3H), 2.65 (s, 1H), 2.51 (s, 3H), 2.32 (s, 3H), 2.26 (d, *J* = 2.6 Hz, 2H), 1.86 – 1.79 (m, 2H), 1.70 – 1.63 (m, 2H). HR-MS (ESI) for $C_{17}H_{21}N_3$ ([M+H]$^+$): 268.1806.

2.7. Synthesis of ATMND-(6-TAMRA) conjugation

2.7.1. Synthesis of N-(4-(1-benzyl-1H-1,2,3-triazol-4-yl)butyl)-5,6,7-trimethyl 1,8-naphthyridin-2-amine 15

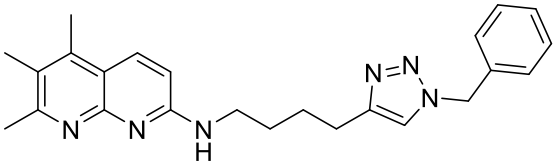

Figure 43. Structure of N-(4-(1-benzyl-1H-1,2,3-triazol-4-yl)butyl)-5,6,7-trimethyl-1,8-naphthyridin-2-amine **15**.

In this case, reactions were done in microscale, so that all starting materials

and reagents were made in solution: alkyne modified ATMND **12** (0.027 g, 0.10 mmol) was dissolved in 10 ml methanol to give 10 mM solution A; (azidomethyl)benzene **14** (0.013 g, 0.10 mmol) was dissolved in 10 ml methanol to give 10 mM solution B; sodium ascorbic acid (0.002 g, 0.01 mmol) was dissolved in 10 ml water to give 1 mM solution C. Solution A 10 ul, solution B 10 ul, solution C 880 ul and 10 mM copper (II)-TBTA in 100% MeOH 100 ul were mixed in an Eppendorf tube. Reaction ran at room temperature for 24 hours under argon protection to give main product N-(4-(1-benzyl-1H-1,2,3-triazol-4-yl)butyl)-5,6,7-trimethyl-1,8-naphthyridin-2-amine **15**. LR-MS ([M+H]$^+$): 401.37.

2.7.2. Synthesis of ATMND-(6-TAMRA) 16

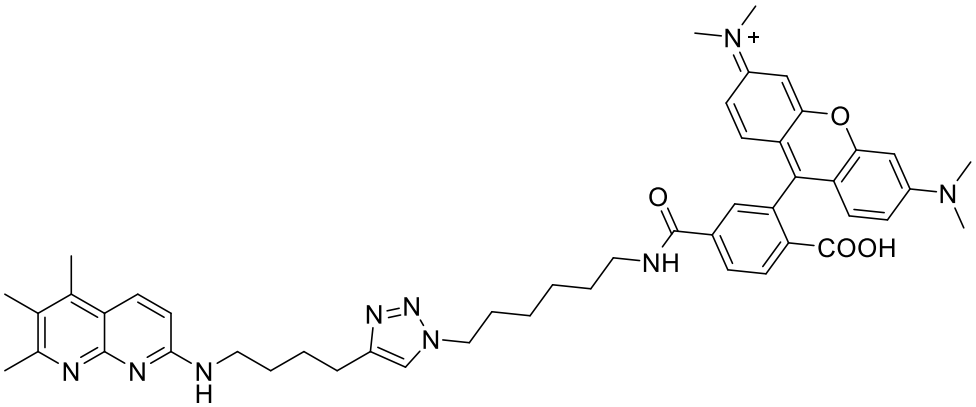

Figure 44. Structure of ATMND-(6-TAMRA) **16**.

The reaction to create ATMND-(6-TAMRA) is similar with synthesis of compound **15**. 6-TAMRA azide 00 (0.003 g, 0.005 mmol) was dissolved in 540 ul methanol to give 10 mM solution D and sodium ascorbic acid (0.002 g, 0.01 mmol) was dissolved in 300 ul water to give solution C. Solution A 50 ul, solution D 50 ul, solution C 150 ul and 20 mM copper (II)-TBTA in 100% MeOH 250 ul were mixed in an Eppendorf tube. Reaction ran at room temperature for 2 days under argon

protection. The desired product ATMND-(6-TAMRA) **16** was separated through TLC plate. LR-MS ($[M+H]^{2+}$): 412.10 ($[M]^{+}$): 822.43.

2.8. Synthesis of ATMND dimer 17

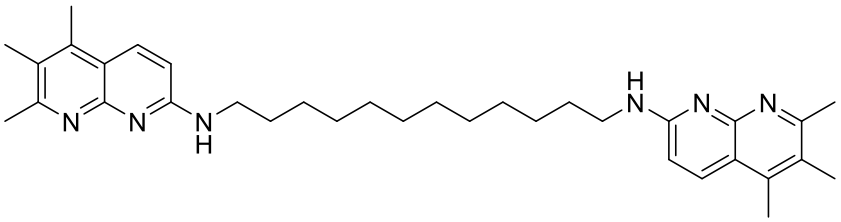

Figure 45. Structure of ATMND dimer **17**.

A mixture of 2-chloro-5,6,7-trimethyl-1,8-naphthyridine **5** (0.04 g, 0.19 mmol) and 1,12-diaminododecane **18** (0.01 g, 0.05 mmol) were dissolved in 0.5 ml methanol. The reaction solution was refluxed at 130°C for 8 hours and then the solvent was removed under reduced pressure. The residue was purified using silica column chromatography (ethyl acetate : methanol=4 :1) to obtain N^{1},N^{12}-bis(5,6,7,-trimethyl-1,8-naphthyridin-2-yl)dodecane-1,12-diamine **17** as yellow gum (0.008 g, 0.015 mmol, 30% yield). ^{1}H-NMR (300MHz, methanol-d4): 8.14 (d, *J* = 9.3 Hz, 2H), 6.88 (d, *J* = 9.2 Hz, 2H), 4.10 (dd, *J* = 14.4, 7.2 Hz, 2H), 3.51 (t, *J* = 6.9 Hz, 4H), 2.66 (s, 6H), 2.61 (s, 6H), 2.35 (s, 6H), 1.28 (s, 20H). LR-MS ($[M+2H]^{2+}$): 271.57 ($[M+H]^{+}$): 541.67.

3. Fluorescence measurement

Fluorescence responses were measured in black 96-well plate using SpectraMAX Gemini XS Microplate Spectrofluorometer at 25°C. Binding affinity of probes was determined by fluorescent titration experiments, in which the concentration of probes was fixed at 1.0 μM and add increasing concentration of

DNA duplexes or hybrid RNA-DNA nanostructures with AP site present or absent. The result titration curves were fit with Growth/Sigmoidal DoseResp function. Titration curves of DNA duplexes with cytosine opposite AP site were formed based on average data points and other curves were formed with single data points.

4. Hybrid RNA-DNA nanostructure preparation

Hybrid RNA-DNA nanostructures were prepared through procedures explored by a previous master Alba Monferrer. Constituent oligonucleotides were dissolved in 10 mM sodium cacodylate buffer (pH 6.5) or 10 mM HEPES buffer (pH 7.0) (only used for Cy5 included samples) and mixed with 2 mM magnesium chloride, then the mixture was incubated at 37°C in Eppendorf tube for 10 minutes before cooled down to room temperature and ligands added.

5. FRET experiments

FRET measurements were performed on a Spectra Max Gemini XS monochromator plate reader (Molecular Devices) at 25°C by exciting the ATMND moiety at 375 nm and recording emission of 6-TAMRA at 610 nm or Cy5 at 670 nm, or by exciting 6-TAMRA moiety at 543 nm and correspondingly recording emission of Cy5. All spectra of these three conjugated fluorophores ATMND, 6-TAMRA and Cy5 were also investigated. Concentrations of these three fluorophores were fixed at 1.0 μM.

6. Gel electrophoresis

Assembly reaction products were electrophoresed on 8% acrylamide/bis acrylamide (19 : 1) native gel (for ATMND as ligand) or 5% acrylamide/bis acrylamide

(19 : 1) native gel (for ATMND-(6-TAMRA) as ligand) in 2X MOPS buffer (40 mM 3-morpholinopropane-1-sulfonic acid, 10 mM sodium acetate) containing 2 mM magnesium chloride. The gels were run for 1 to 3 hours at 220 V, 22 mA. Visualization was performed under UV light after ethidium bromide staining.

Appendix

Spectrum A1. LR-MS ESI Positive Ion Mode of compound **1** (ATMND).

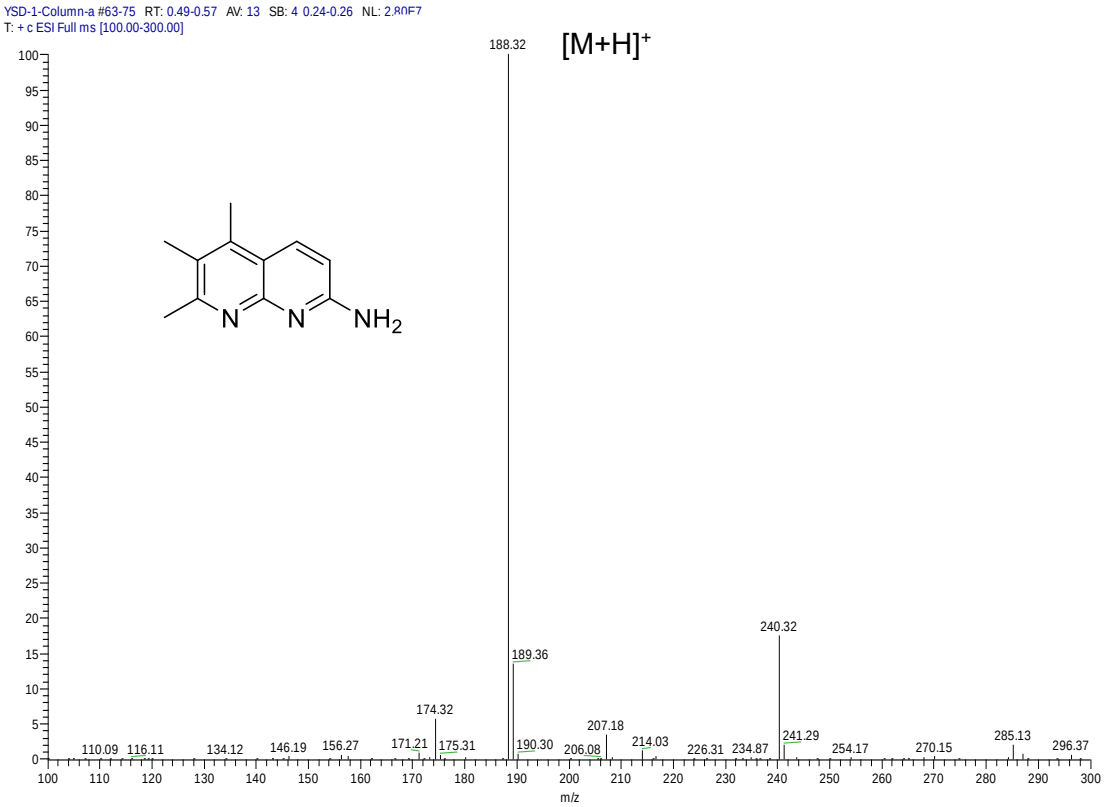

Spectrum A2. ^{1}H-NMR of compound **1** (300MHz, Methanol-d4).

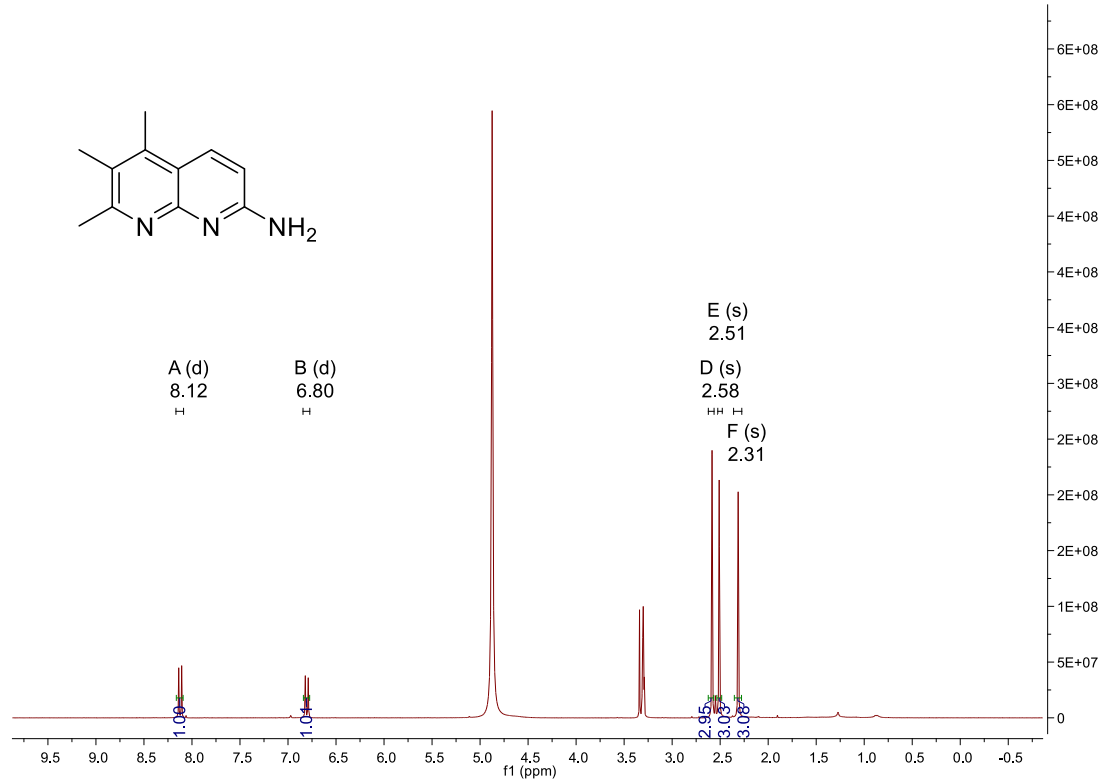

Spectrum A3. LR-MS ESI Positive Ion Mode of compound **5.**

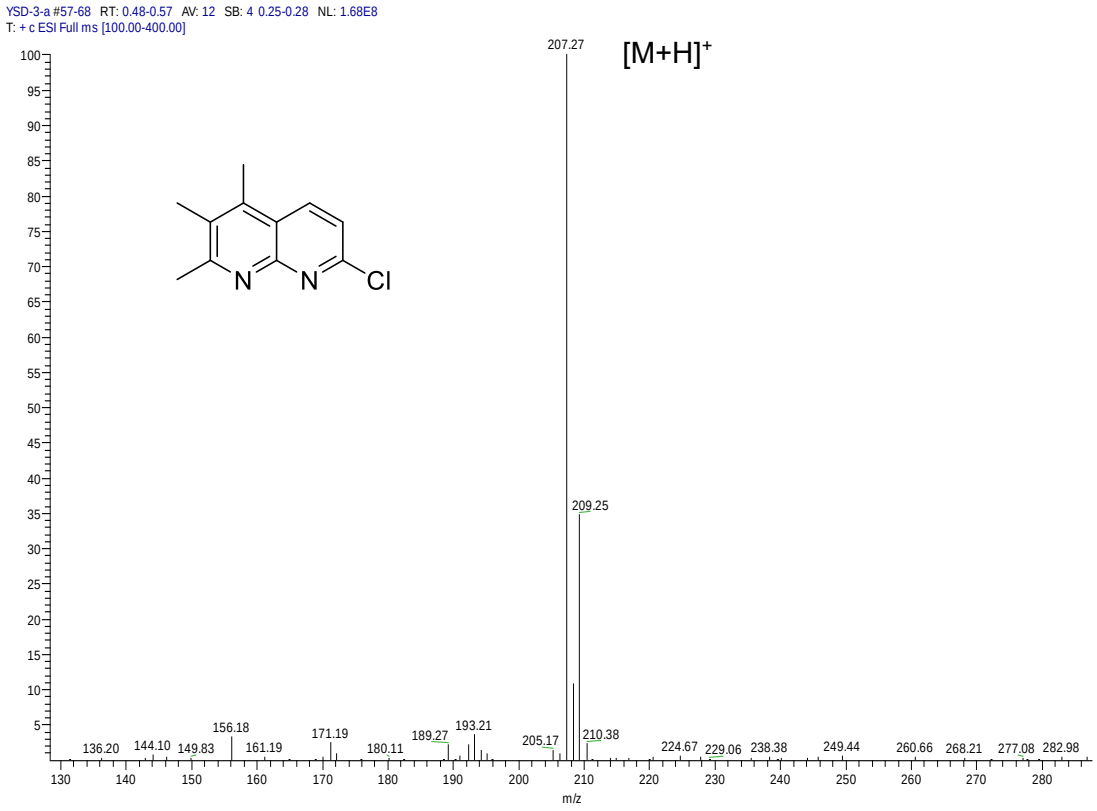

Spectrum A4. ^{1}H-NMR of compound **5** (300MHz, Methanol-d4).

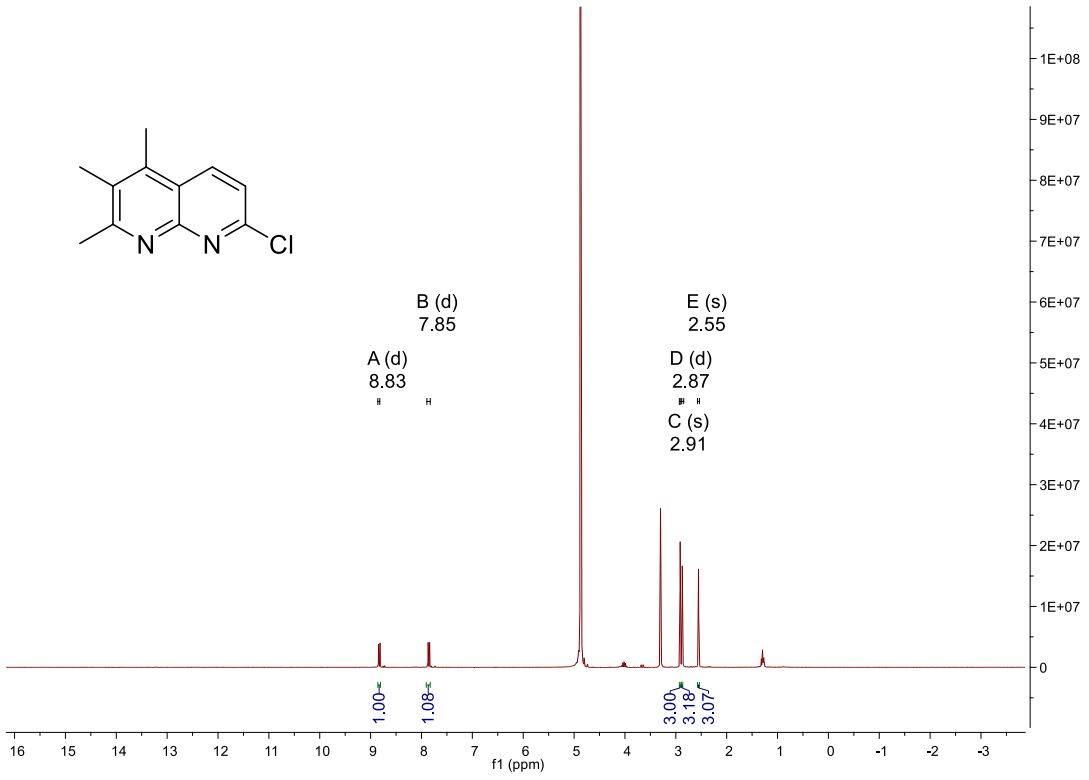

Spectrum A5. HR-MS ESI Positive Ion Mode of compound **6.**

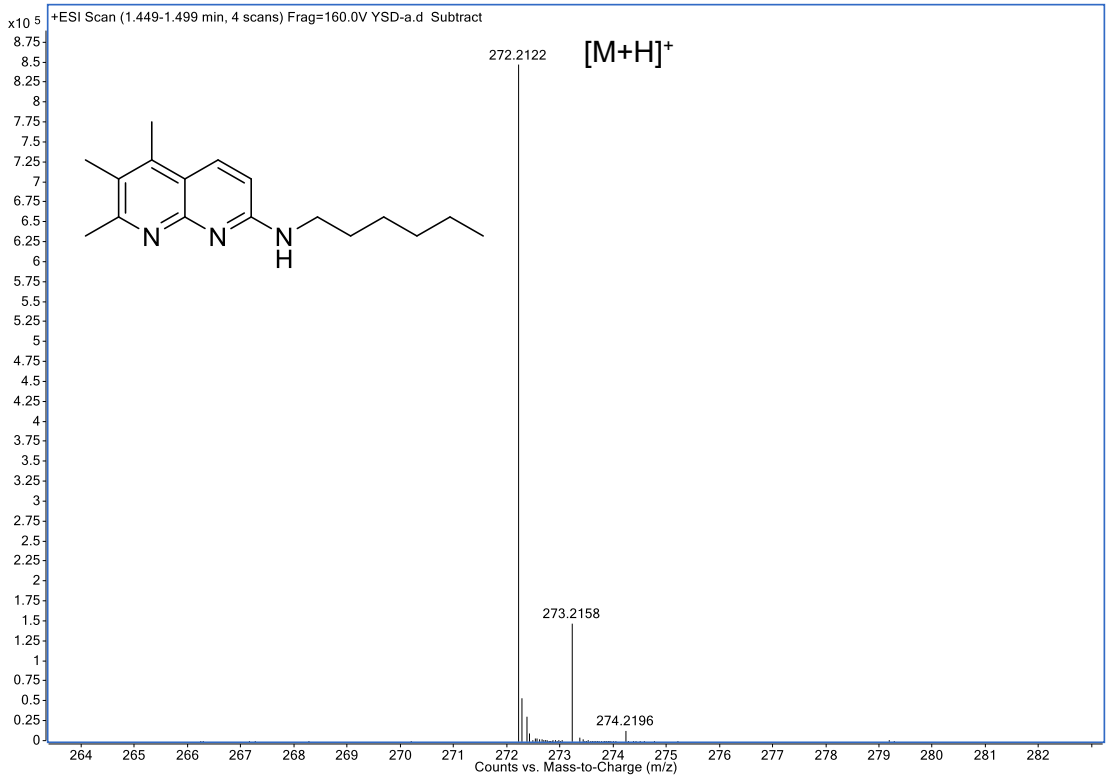

Mass Measured	Theo. Mass	Delta (ppm)	Composition
272.2122	272.2121	0.4	$[C_{17}\ H_{26}\ N_3]^+$

Spectrum A6. ^{1}H-NMR of compound **6** (300MHz, Methanol-d4).

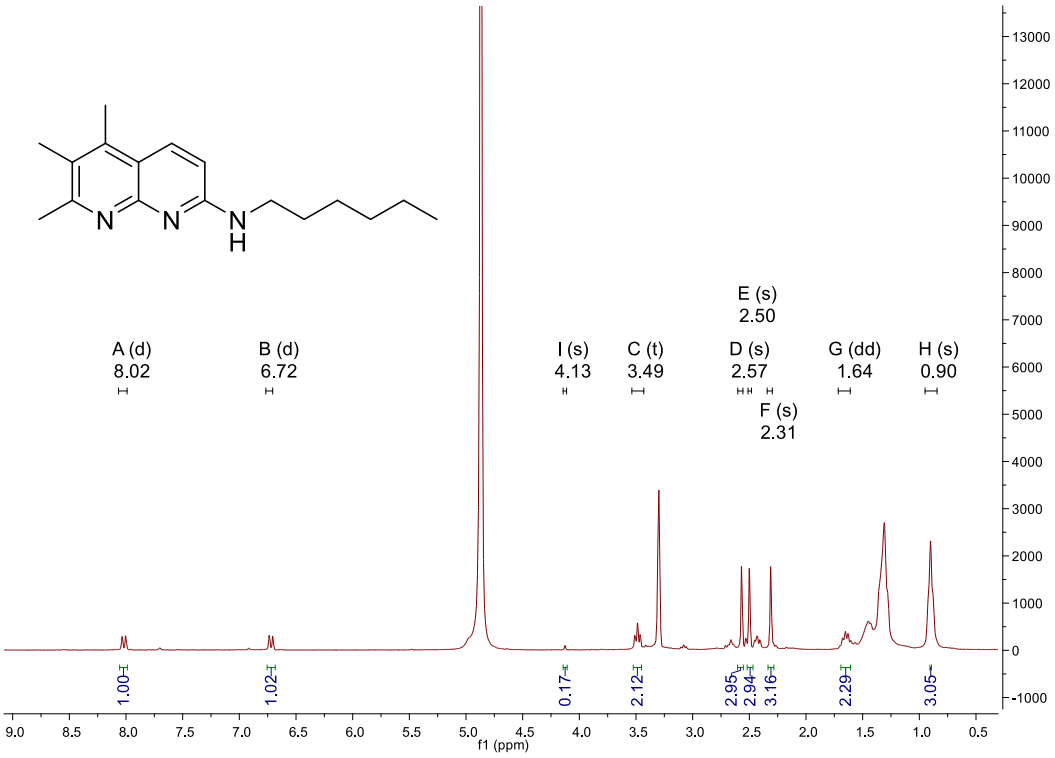

Spectrum A7. LR-MS ESI Positive Ion Mode of compound **9.**

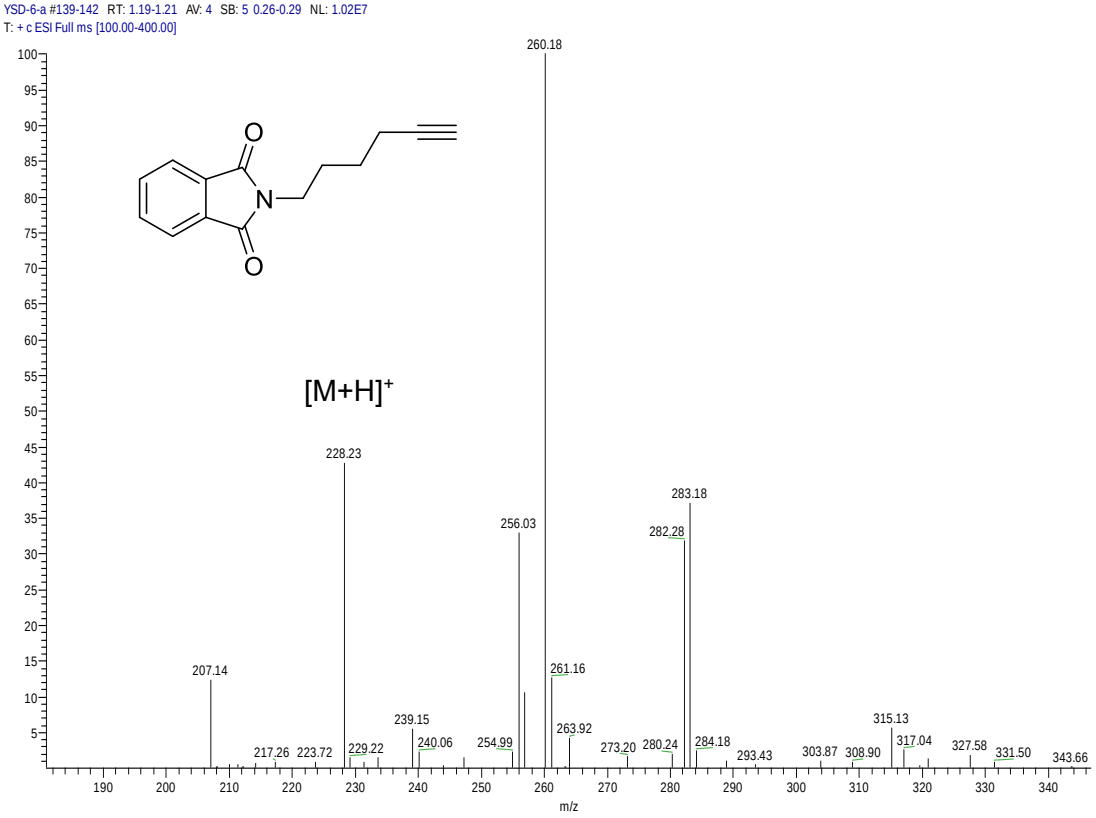

Spectrum A8. ^{1}H-NMR of compound **9** (300MHz, chloroform-d4).

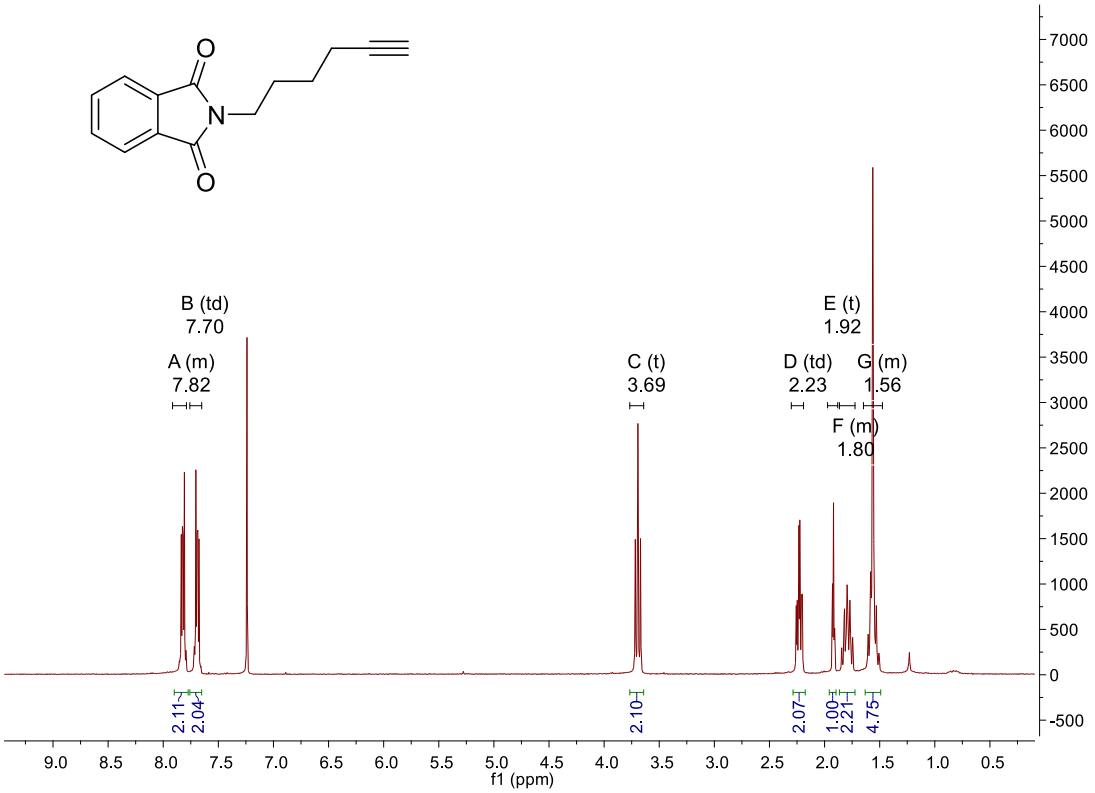

Spectrum A9. LR-MS ESI Positive Ion Mode of compound **8.**

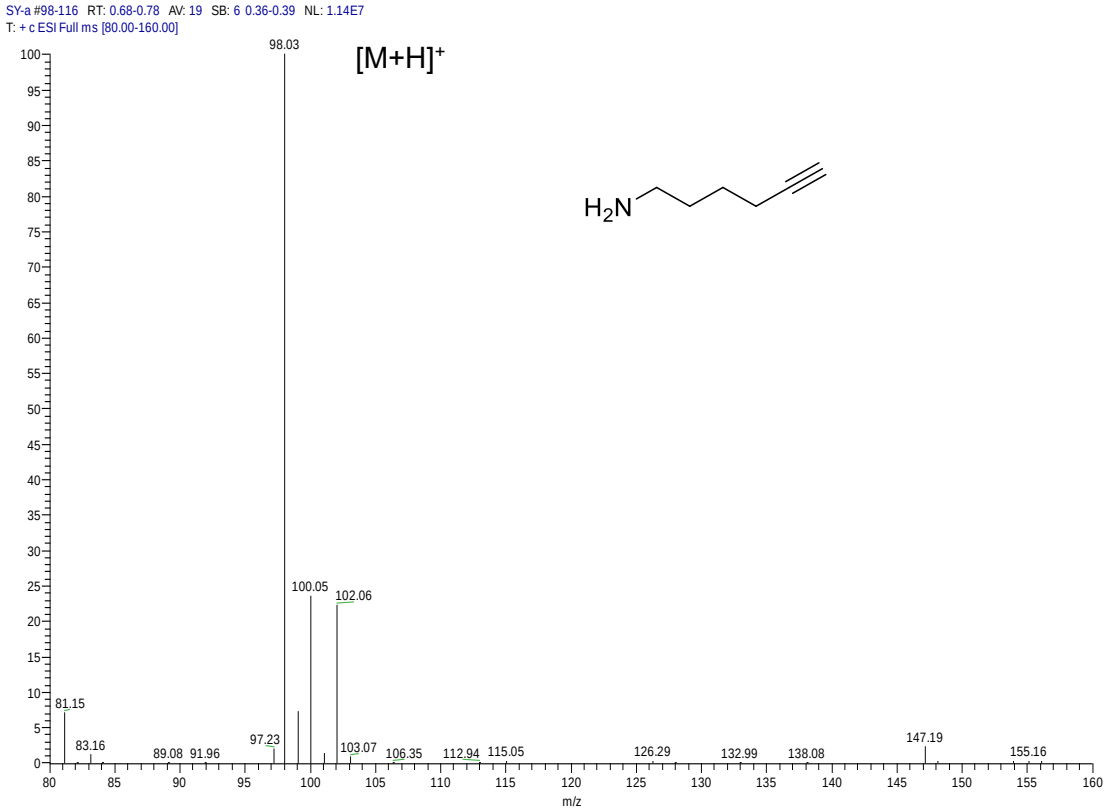

Spectrum A10. ^{1}H-NMR of compound **8** (300MHz, chloroform-d4).

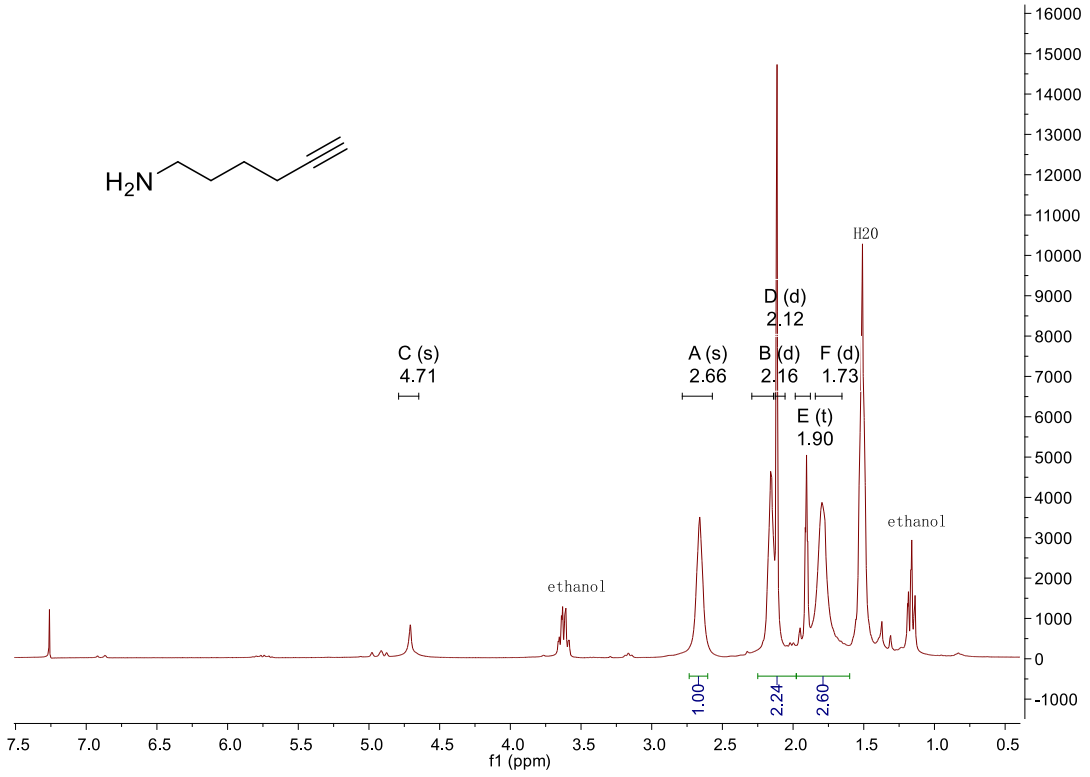

Spectrum A11. HR-MS ESI Positive Ion Mode of compound **12.**

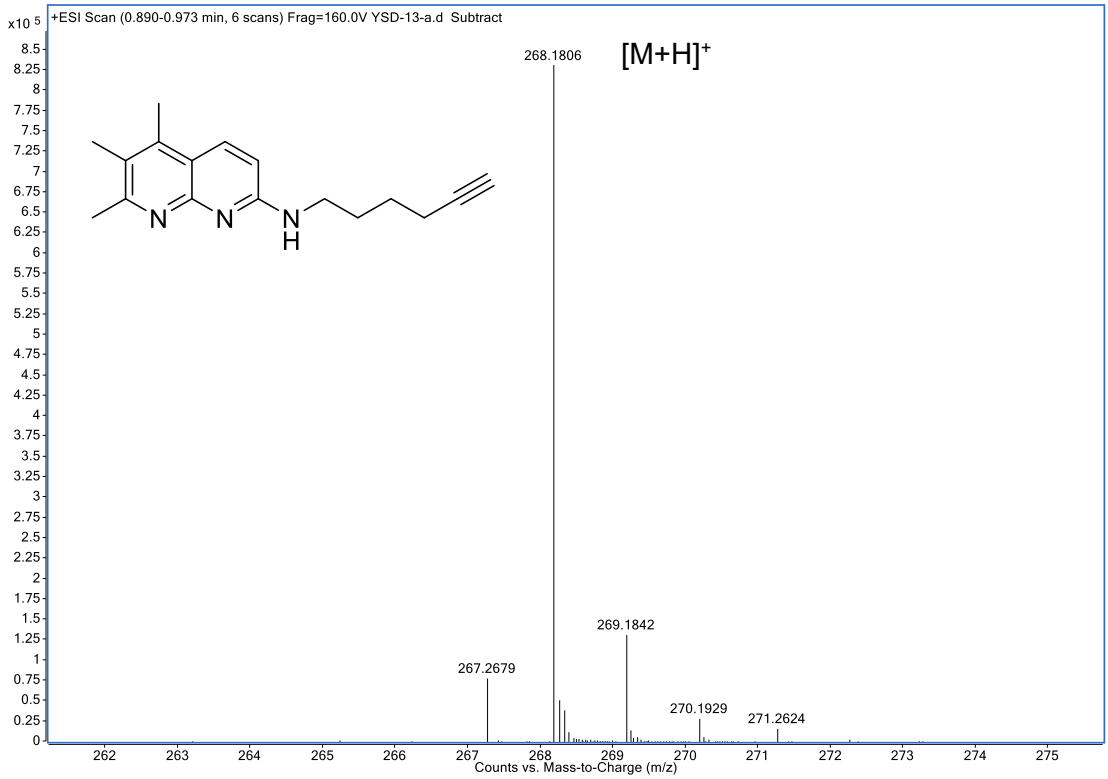

Mass Measured	Theo. Mass	Delta (ppm)	Composition
268.1806	268.1808	-0.7	$[C_{17}H_{22}N_3]^+$

Spectrum A12. ^{1}H-NMR of compound **12** (300MHz, chloroform-d4).

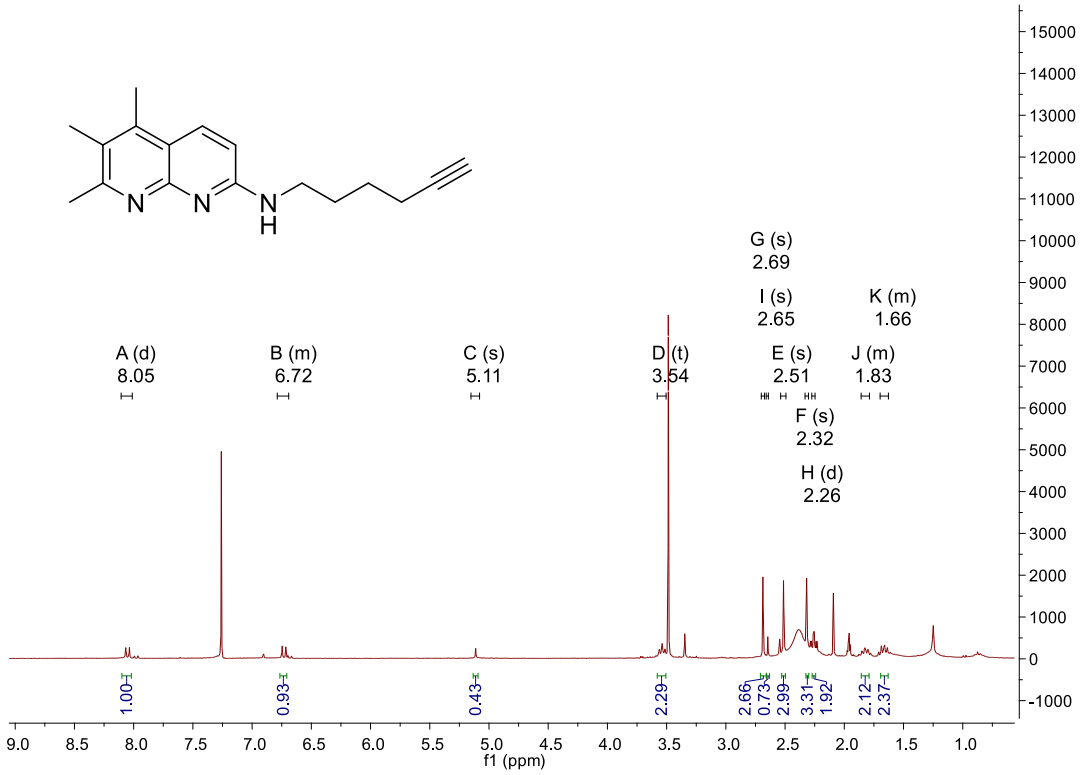

Spectrum A13. LR-MS ESI Positive Ion Mode of compound **15.**

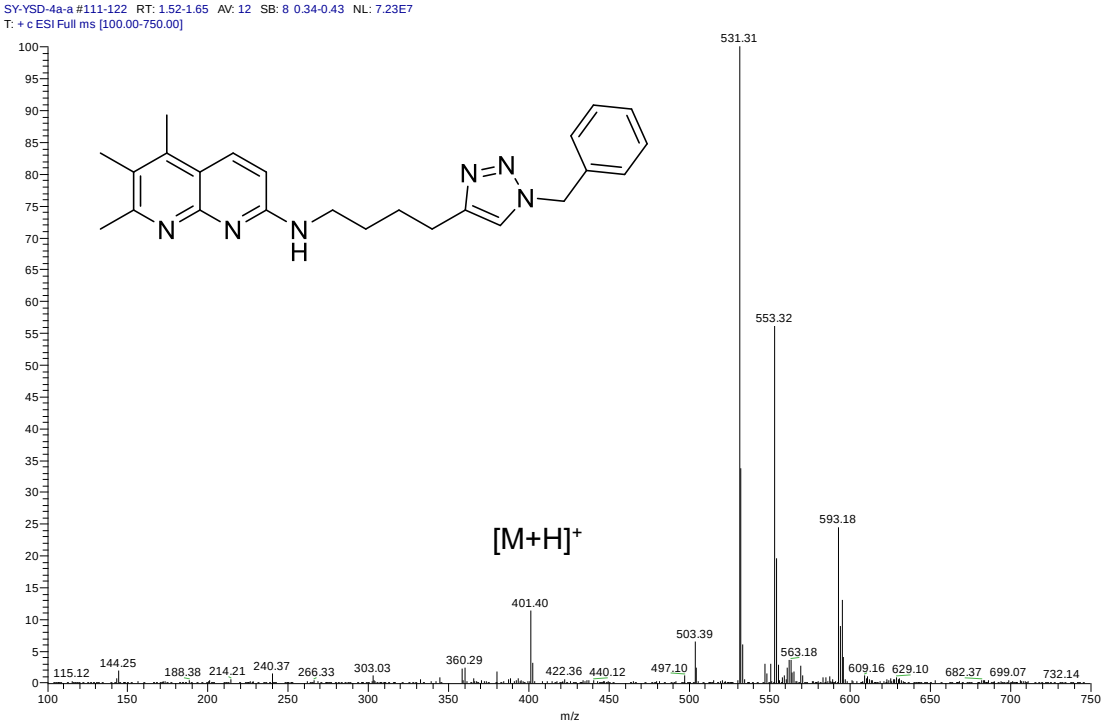

Spectrum A14. LR-MS ESI Positive Ion Mode of compound **16.**

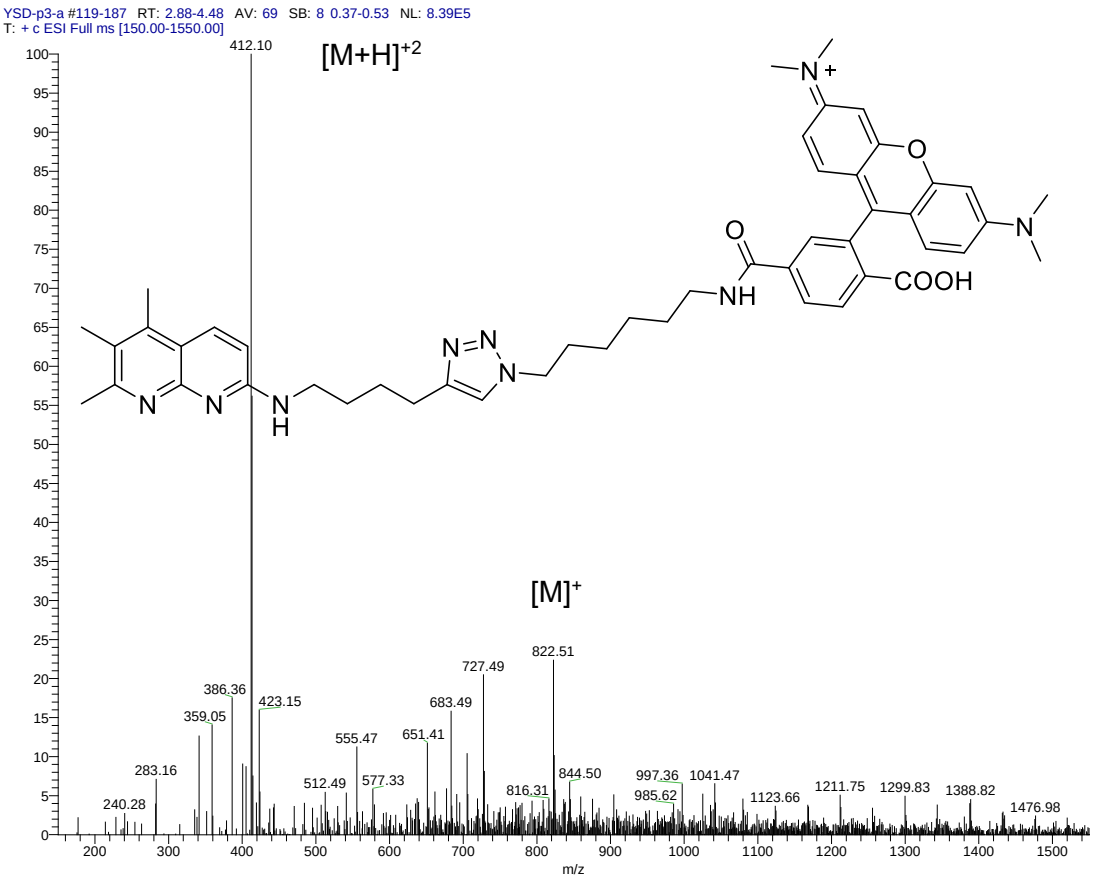

Spectrum A15. HR-MS ESI Positive Ion Mode of compound **17.**

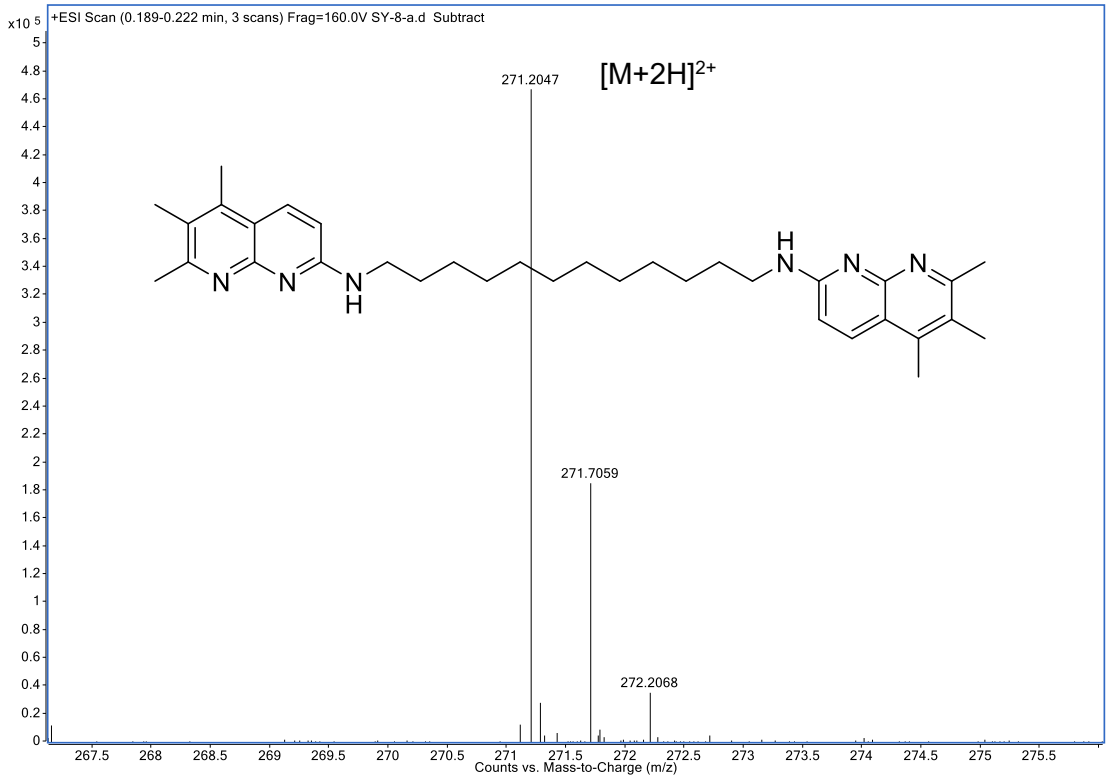

Mass Measured	Theo. Mass	Delta (ppm)	Composition
286.1107	286.1108	-0.3	$[C_{13}H_{16}O_4SNH_4]^+$

Spectrum A16. ^{1}H-NMR of compound **17** (300MHz, Methanol-d4).

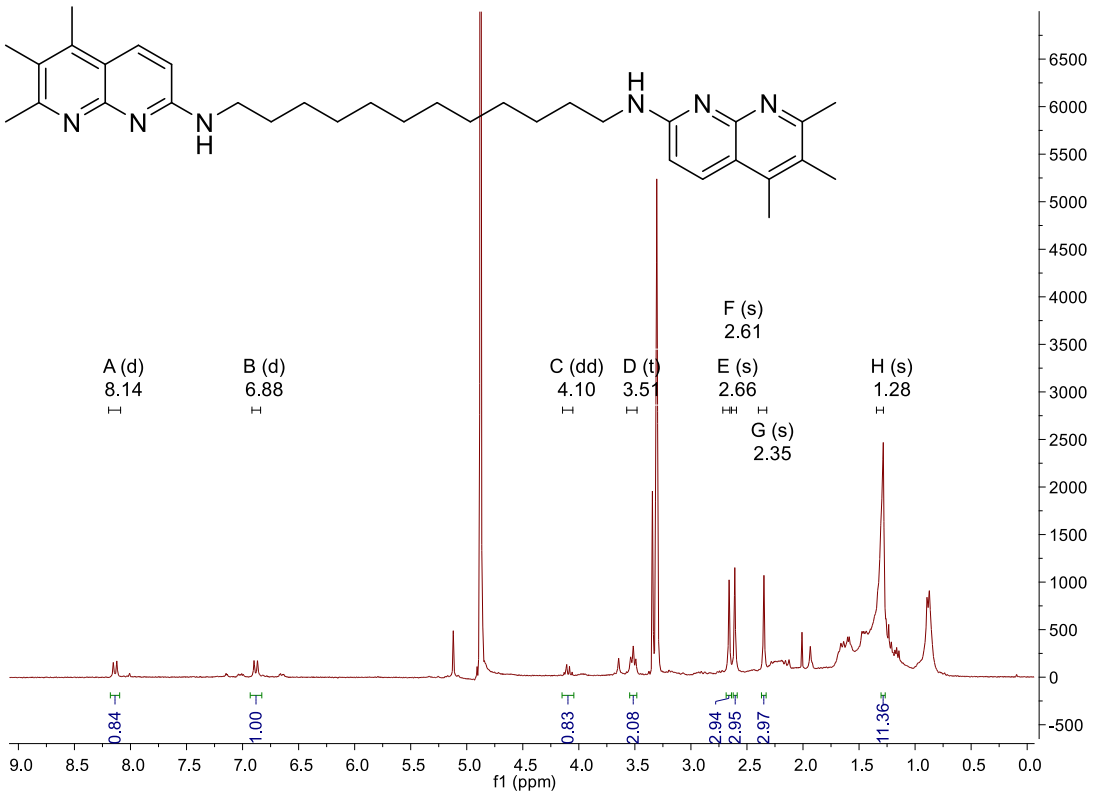

Table A1. DNA oligonucleotides sequences used in this project.

SY-T-In-23	5’ - GTC TCG TAT CGT CAC GT CCG AGG - 3’
SY-T-Out-23	5’ - CCT CGG ACG TGA CGA TA CGA GAC - 3’
SY-C-In-23	5’ - GTC TCG TAT CGC CAC GT CCG AGG - 3’
SY-C-Out-23	5’ - CCT CGG ACG TGG CGA TA CGA GAC - 3’
SY-A-In-23	5’ - GTC TCG TAT CGA CAC GT CCG AGG - 3’
SY-A-Out-23	5’ - CCT CGG ACG TGT CGA TA CGA GAC - 3’
SY-G-In-23	5’ - GTC TCG TAT CGG CAC GT CCG AGG - 3’
SY-G-Out-23	5’ - CCT CGG ACG TGC CGA TA CGA GAC - 3’
SY-AP-Out-23	5’ - CCT CGG ACG TG/idSp/ CGA TA CGA GAC - 3’
SY-C-In-17	5’ - GTC TCG TAT CGC CAC GT - 3’
SY-C-Out-17	5’ - CCT CGG ACG TGG CGA TA - 3’
SY-AP-Out-17	5’ - CCT CGG ACG TG/idSp/ CGA TA - 3’
SY-C-In-27	5’ - GTC TCG TGC ACT CGA TTA TCG CTA CGT - 3’
SY-C-Out-27	5’ - CCT CGG ACG TAG CGA TAA TCG AGT GCA - 3’
SY-AP-Out-27	5’ - CCT CGG ACG TAG C/idSp/A TAA TCG AGT GCA - 3’
TU4-11-In	5’ - TTT GTC TCG TAT CGC TAC GTT TTC TCT CTC TCT TTT GTC TCG TAT CGC TAC GTT TTC TCT CTC TCT TTT GTC TCG TAT CGC TAC GTT TTC TCT CTC TCT TTT GTC TCG TAT CGC TAC GTT TT - 3’

Table A2. RNA oligonucleotides sequences used in this project.

AR-In	5’ - rCrCrG rArGrG rUrCrA rGrCrC rUrG - 3’
AR-Out	5’ - rCrGrA rGrArC rCrArG rGrArA rCrUrA rCrUrG rA - 3’
AR-Out-Cy5	5’ - (Cy5) rCrGrA rGrArC rCrArG rGrArA rCrUrA rCrUrG rA - 3’
HCV-Sq-In	5’ - rCrCrG rGrCrA rGrCrC rU - 3’
HCV-Sq-Out	5’ - rCrCrG rGrArG rGrArA rCrUrA rCrUrG - 3’

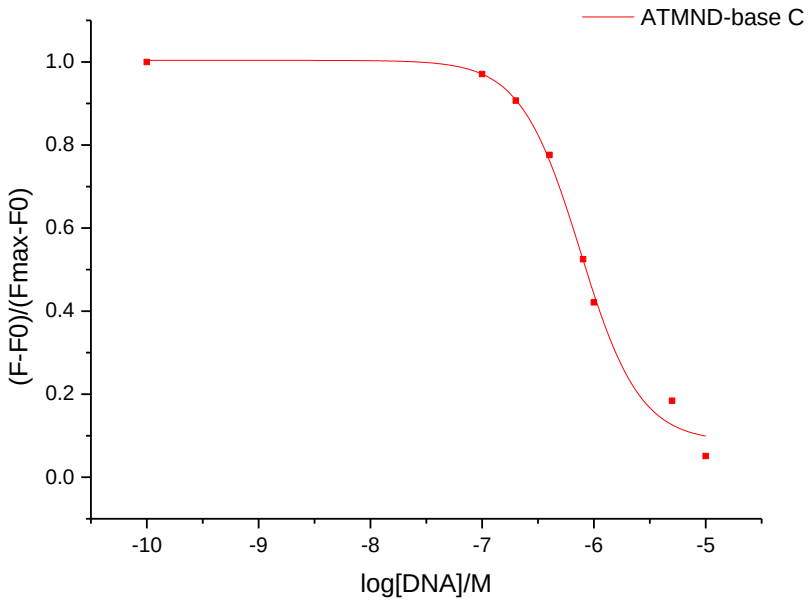

Figure A1. Fluorescence responses of ATMND (1 μM) to cytosine in **17**-meric AP site-containing DNA duplexes (In strand: SY-C-In-**17**; Out strand: SY-AP-Out-**17**) in solutions buffered to pH 6.5 (10 mM sodium cacodylate) and containing $MgCl_2$ 2 mM. *T*=room temperature.

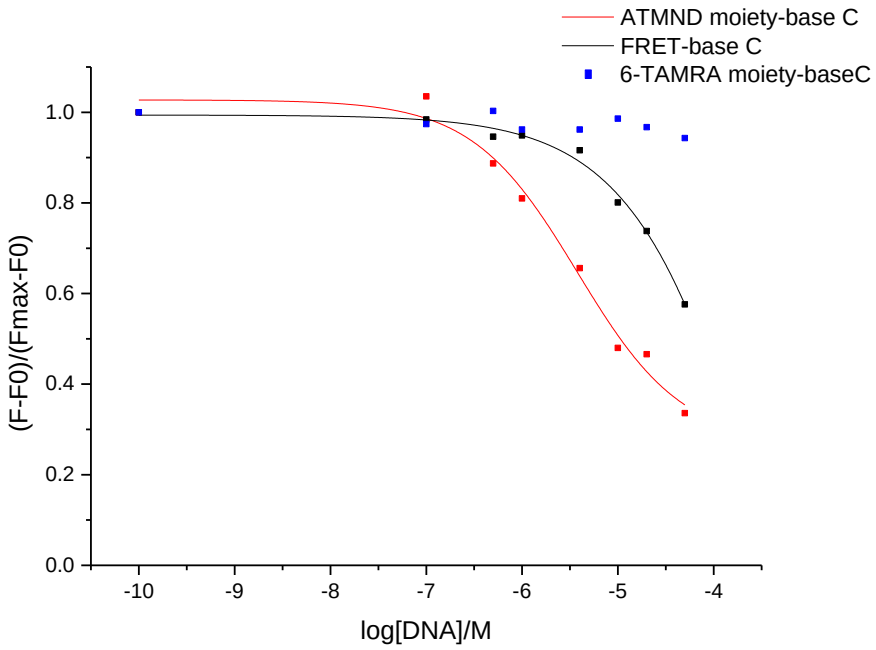

Figure A2. Fluorescence responses of ATMND-(6-TAMRA) (1 μM) to cytosine in **17**-meric AP site-containing DNA duplexes (In strand: SY-C-In-**17**; Out strand: SY-AP-Out-**17**) in solutions buffered to pH 6.5 (10 mM sodium cacodylate) and containing $MgCl_2$ 2 mM. *T*=room temperature.

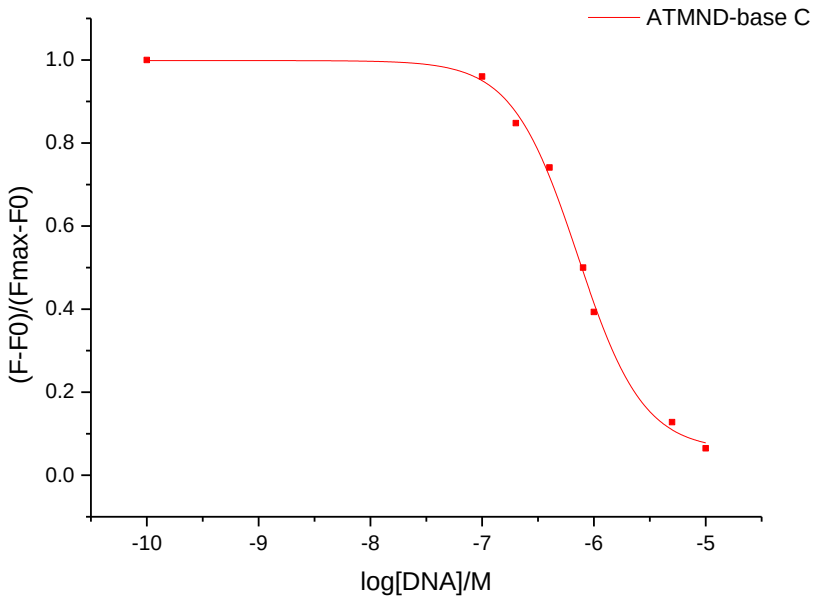

Figure A3. Fluorescence responses of ATMND (1 μM) to cytosine in **27**-meric AP site-containing DNA duplexes (In strand: SY-C-In-**27**; Out strand: SY-AP-Out-**27**) in solutions buffered to pH 6.5 (10 mM sodium cacodylate) and containing $MgCl_2$ 2 mM. *T*=room temperature.

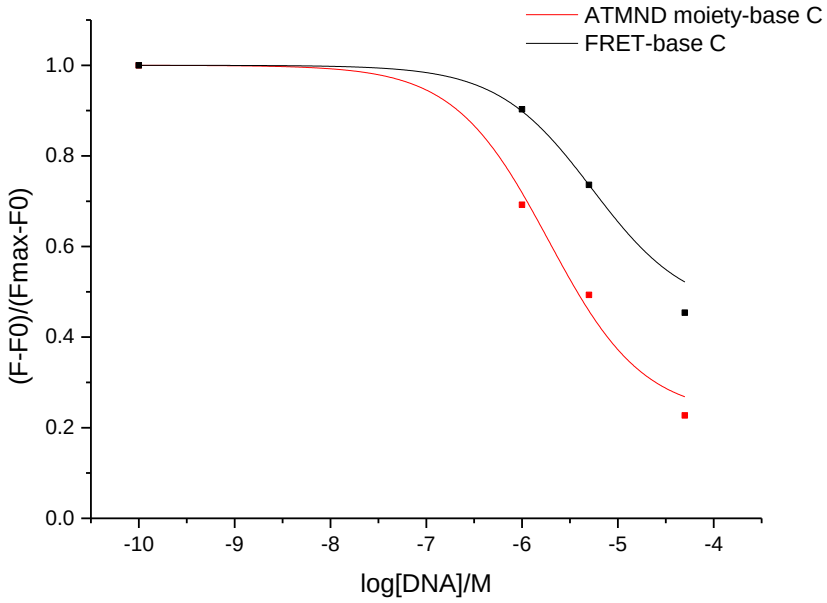

Figure A4. Fluorescence responses of ATMND-(6-TAMRA) (1 μM) to cytosine in **27**-meric AP site-containing DNA duplexes (In strand: SY-C-In-**27**; Out strand: SY-AP-Out-**27**) in solutions buffered to pH 6.5 (10 mM sodium cacodylate) and containing $MgCl_2$ 2 mM. *T*=room temperature.

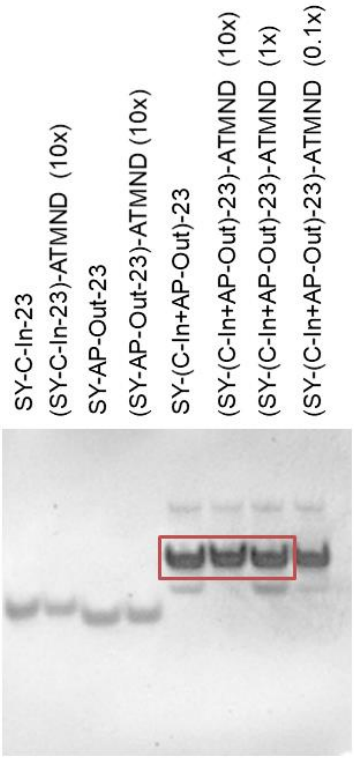

Figure A5. Interaction of ATMND ligand with AP site-containing DNA duplexes (23 base pairs, **N**=C) (10% native PAGE containing 2 mM $MgCl_2$).

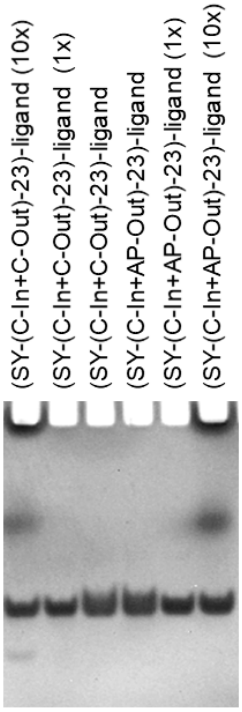

Figure A6. Interaction of ATMND-(6-TAMRA) ligand with AP site-containing DNA duplexes (23 base pairs, **N**=C) (8% native PAGE containing 2 mM $MgCl_2$). ligand=ATMND-(6-TAMRA).

References

1. Boiteux S, Guillet M. Abasic sites in DNA: repair and biological consequences in Saccharomyces cerevisiae. DNA repair. 2004;3(1):1-12.

2. Krokan HE, Bjoras M. Base excision repair. Cold Spring Harbor perspectives in biology. 2013;5(4):a012583.

3. Talpaert-Borle M. Formation, detection and repair of AP sites Mutation Research. 1987;181.

4. Jean Lhomme J-FoC, Martine Demeunynck Abasic DNA Structure, Reactivity, and Recognition. Biopolymers. 1999;52.

5. Hrdlicka PJ, Karmakar S. 25 years and still going strong: 2'-O-(pyren-1-yl)methylribonucleotides - versatile building blocks for applications in molecular biology, diagnostics and materials science. Organic & biomolecular chemistry. 2017;15(46):9760-74.

6. Naskar S, Guha R, Muller J. Metal-Modified Nucleic Acids: Metal-Mediated Base Pairs, Triples, and Tetrads. Angewandte Chemie. 2020;59(4):1397-406.

7. Jash B, Muller J. Metal-Mediated Base Pairs: From Characterization to Application. Chemistry. 2017;23(68):17166-78.

8. Tuerk C, Gold L. Systematic Evolution of Ligands by Exponential Enrichment: RNA Ligands to Bacteriophage T4 DNA Polymerase. Science. 1990;249.

9. Hermann T, Patel DJ. Adaptive Recognition by Nucleic Acid Aptamers Science. 2000;287.

10. Haq I, Ladbury J. Drug-DNA Recognition: energetics and implications for design. JOURNAL OF MOLECULAR RECOGNITION 2000;13.

11. Yoshimoto K, Nishizawa S, Minagawa M, Teramae N. Use of Abasic Site-Containing DNA Strands for Nucleobase Recognition in Water. J AM CHEM SOC. 2003;125.

12. Zhao C, Dai Q, Seino T, Cui YY, Nishizawa S, Teramae N. Strong and selective binding of amiloride to thymine base opposite AP sites in DNA duplexes: simultaneous binding to DNA phosphate backbone. Chemical communications. 2006(11):1185-7.

13. Dai Q, Xu C, Sato Y, Yoshimoto K, Nishizawa S, Teramae N. Enhancement of the Binding Ability of a Ligand for a Nucleobase Recognition by Introducing a Methyl Group. ANALYTICAL SCIENCES. 2006;22.

14. Rajendar B, Nishizawa S, Teramae N. Alloxazine as a ligand for selective binding to adenine opposite AP sites in DNA duplexes and analysis of single-nucleotide polymorphisms. Organic & biomolecular chemistry. 2008;6(4):670-3.

15.Nishizawa S, Sankaran NB, Seino T, Cui Y-Y, Dai Q, Xu C-Y, Yoshimoto K, Teramae N. Use of vitamin B2 for fluorescence detection of thymidine-related single-nucleotide polymorphisms. Analytica Chimica Acta. 2006;556(1):133-9.

16.Rajendar B, Rajendran A, Ye Z, Kanai E, Sato Y, Nishizawa S, Sato Y, Sikorski M, Teramae N. Effect of substituents of alloxazine derivatives on the selectivity and affinity for adenine in AP-site-containing DNA duplexes. Organic & biomolecular chemistry. 2010;8(21):4949.

17.Sato Y, Nishizawa S, Yoshimoto K, Seino T, Ichihashi T, Morita K, Teramae N. Influence of substituent modifications on the binding of 2-amino-1,8-naphthyridines to cytosine opposite an AP site in DNA duplexes: thermodynamic characterization. Nucleic acids research. 2009;37(5):1411-22.

18.Fu X, Peng F, Lee J, Yang Q, Zhang F, Xiong M, Kong G, Hong MM, Ke G, Zhang XB. Aptamer-Functionalized DNA Nanostructures for Biological Applications. Topics in current chemistry. 2020;378(2):21.

19.Chao J, Lin Y, Liu H, Wang L, Fan C. DNA-based plasmonic nanostructures. Materials Today. 2015;18(6):326-35.

20.Zhang L, Yang Y, Tan J, Yuan Q. Chemically modified nucleic acid biopolymers used in biosensing. Materials Chemistry Frontiers. 2020.

21.Jasinski D, Haque F, Binzel DW, Guo P. Advancement of the Emerging Field of RNA Nanotechnology. ACS nano. 2017;11(2):1142-64.

22.Khisamutdinov EF, Li H, Jasinski DL, Chen J, Fu J, Guo P. Enhancing immunomodulation on innate immunity by shape transition among RNA triangle, square and pentagon nanovehicles. Nucleic acids research. 2014;42(15):9996-10004.

23.Dibrov SM, McLean J, Parsons J, Hermann T. Self-assembling RNA square PNAS. 2011;108.

24.Ko SH, Su M, Zhang C, Ribbe AE, Jiang W, Mao C. Synergistic self-assembly of RNA and DNA molecules. Nature chemistry. 2010;2(12):1050-5.

25.Monferrer A, Zhang D, Lushnikov AJ, Hermann T. Versatile kit of robust nanoshapes self-assembling from RNA and DNA modules. Nature communications. 2019;10(1):608.

26.Xu Z, Morita K, Sato Y, Dai Q, Nishizawa S, Teramae N. Label-free aptamer-based sensor using abasic site-containing DNA and a nucleobase-specific fluorescent ligand. Chemical communications. 2009(42):6445-7.

27.Sato Y, Kudo M, Toriyabe Y, Kuchitsu S, Wang CX, Nishizawa S, Teramae N. Abasic site-binding ligands conjugated with cyanine dyes for "off-on" fluorescence sensing of orphan nucleobases in DNA duplexes and DNA-RNA hybrids. Chemical communications. 2014;50(5):515-7.

28.Wang CX, Sato Y, Kudo M, Nishizawa S, Teramae N. Ratiometric Fluorescent Signaling of Small Molecule Environmentally Sensitive Dye Conjugate for Detecting Single-Base Mutations in DNA. Chemistry-A European Jornal. 2012;18(31).

29.Hauser CR, Weiss MJ. CYCLIZATION OF 2-AMINOPYRIDINE DERIVATIVES TO FORM 1,8-NAPHTHYRIDINES Journal of Organic Chemistry. 1949;14.

30.Li X, Xiong M, Huang Y, Zhang L, Zhao S. Simple label-free fluorescence detection of apurinic/apyrimidinic endonuclease 1 activity and its inhibitor using the abasic site-binding fluorophore. Analytical Methods. 2019;11(6):739-43.

31.Brown EV. 1,8-Naphthyridines. I. Derivatives of 2- and 4-Methyl-l,8-naphthyridines Journal of Organic Chemistry. 1965;30(5).

32.Ichihashi T, Sato Y, Seino T, Nishizawa S, Teramae N. Effect of an alkyl amino group on the binding of 1,8-naphthyridines to AP site-containing DNA duplexes. Nucleic acids symposiμM series. 2008(52):117-8.

33.Sato Y, Rokugawa M, Ito S, Yajima S, Sugawara H, Teramae N, Nishizawa S. Fluorescent Trimethylated Naphthyridine Derivative with an Aminoalkyl Side Chain as the Tightest Non-aminoglycoside Ligand for the Bacterial A-site RNA. Chemistry. 2018;24(52):13862-70.

34.Pouy MJ, Delp SA, Uddin J, Ramdeen VM, Cochrane NA, Fortman GC, Gunnoe TB, Cundari TR, Sabat M, Myers WH. Intramolecular Hydroalkoxylation and Hydroamination of Alkynes Catalyzed by Cu(I) Complexes Supported by N-Heterocyclic Carbene Ligands. ACS Catalysis. 2012;2(10):2182-93.

35.Kikuchi K. Design, synthesis and biological application of chemical probes for bio-imaging. Chemical Society reviews. 2010;39(6):2048-53.

36.Yang M, Moroz P, Jin Z, Budkina DS, Sundrani N, Porotnikov D, Cassidy J, Sagiyama Y, Tarnovsky AN, Mattoussi H. Delayed PhotolμMinescence in Metal-Conjugated Fluorophores. Journal of the American Chemical Society. 2019;141(28):11286-97.

37.Keller M, Weiss S, Hutzler C, Kuhn KK, Mollereau C, Dukorn S, Schindler L, Bernhardt G, Konig B, Buschauer A. N(omega)-Carbamoylation of the Argininamide Moiety: An Avenue to Insurmountable NPY Y1 Receptor Antagonists and a Radiolabeled Selective High-Affinity Molecular Tool ([(3)H]UR-MK299) with Extended Residence Time. Journal of medicinal chemistry. 2015;58(22):8834-49.

38.Kusamoto H, Kikuta EK, Nishimura T, Nagai T, Kinoshita E, Koike T. Gel-based analysis of protein phosphorylation status by rapid fluorometric staining using TAMRA-labeled Phos-tag. J Electrophoresis. 2019;63.

39.Kim E, Koo H. Biomedical applications of copper-free click chemistry: in vitro, in vivo, and ex vivo. Chemical science. 2019;10(34):7835-51.

40. Speers AE, Cravatt BF. Profiling enzyme activities in vivo using click chemistry methods. Chemistry & biology. 2004;11(4):535-46.

41. Ordonez YF, Abad JL, Aseeri M, Casas J, Garcia V, Casasampere M, Schuchman EH, Levada T, Delgado A, Triola G, Fabrias G. Activity-Based Imaging of Acid Ceramidase in Living Cells. Journal of the American Chemical Society. 2019;141(19):7736-42.

42. Li X, Kapoor TM. An approach to profile proteins that recognize post-translationally modified histone'tails' Journal of the American Chemical Society. 2010;132(8).

43. Nulwala H, Burke DJ, Khan A, Serrano A, Hawker CJ. N-Vinyltriazoles: A New Functional Monomer Family through Click Chemistry. Macromolecules. 2010;43(12):5474-7.

44. Sato Y, Saito H, Aoki D, Teramae N, Nishizawa S. Lysine linkage in abasic site-binding ligand-thiazole orange conjugates for improved binding affinity to orphan nucleobases in DNA/RNA hybrids. Chemical communications. 2016;52(100):14446-9.

45. Lee GH, Lee EJ, Hah SS. TAMRA- and Cy5-labeled probe for efficient kinetic characterization of caspase-3. Analytical biochemistry. 2014;446:22-4.

46. Chen S, Hermann T. RNA-DNA hybrid nanoshapes that self-assemble dependent on ligand binding. Nanoscale. 2020;12(5):3302-7.